## ABSTRACT

ZHOU, TIANBIN. Bicomponent Nano-fibrous Complexes via Co-axial Electrospinning. (Under the direction of Dr. Wendy E. Krause (TE) and Dr. C. Maurice Balik (MSE)).

Electrospinning is an electro-statically driven method of fabricating fibers at nano/micro-scale. In this work, chitosan, a biocompatible polysaccharide, and poly(acrylic acid) (PAA) were used as a core and sheath materials respectively, to create fibrous complexes via co-axial electrospinning. The purpose of creating such bicomponent materials is to maintain structural integrity of polyelectrolytes in water via electrostatic attraction.

An electrospinable PAA/dimethylformamide (DMF) solution was consistently used as sheath solution to induce the difficult-to-spin chitosan solution in core. Two attempts with dilute hydrochloric acid (dHCl) and 30% aqueous formic acid (30FA) as core solvents successfully formed fibers. Scanning electron microscopy (SEM) revealed that when 30FA was used as core solvent, the electrospun fibers appeared relatively uniform, whereas incomplete evaporation resulted in a film-like mat in the dHCl system. Soaking the two mats in water, the surviving complexes originally derived from dHCl swelled, showing coexistence of solid films along with porous matrix at the nano-scale. The one derived from 30FA maintained a fibrous structure covered with nano-beads. Compared with traditional thermal induced phase transformation for creating hydrogels, this novel approach may be prove to be a more efficient and straightforward method of fabricating controllable porous complexes at the nanoscale.

# Bi-component Nano-fibrous Complexes via Coaxial Electrospinning

by
Tianbin Zhou

A thesis submitted to the Graduate Faculty of
North Carolina State University
in partial fulfillment of the
requirements for the degree of
Master of Science

Textile Engineering
Material Science & Engineering

Raleigh, North Carolina

2011

APPROVED BY:

| | |
|---|---|
| Dr. Wendy E. Krause<br>(Co-Chair of Advisory Committee) | Dr. C. Maurice Balik<br>(Co-Chair of Advisory Committee) |
| Dr. Samuel M. Hudson<br>(Committee Member) | Dr. Russell E. Gorga<br>(Committee Member) |

## BIOGRAPHY

Tianbin Zhou was born in Nanjing, China on December, 1986. Thanks to his family being made up of chemists, he was fascinated with physical science at an early age. After attending a high school affiliated with Nanjing Normal University, he enrolled at Nanjing University of Technology in 2005. While majoring Light Chemical Engineering, he received NJUT-BASF and Sinopec scholarships for excellent academic performance.

In the August of 2009, he began his master studies at North Carolina State University, Raleigh where he majored in Textile Engineering and Material Science. After graduation, he will work for a biotechnology company in Piscataway, NJ to expand his horizons in industry.

## ACKNOWLEDGMENTS

I would like to thank my advisor, Dr. Wendy Krause, for her guidance and encouragement throughout my study. I would also wish to express my appreciation to Dr. C. Maurice Balik, the co-chair of my committee, for his helpful discussions, as well as my committee members Dr. Sam Hudson and Dr. Russell Gorga.

I would like to recognize my research group fellows, Avinav Nandgaonkar, Nagarajan Muthuraman and Dr. Rebecca Klossner for all of their contributions to the success of my work. I would also like to express thanks to Dr. Birgit Anderson and Ms. Judy Elson for their help with analytical instrumentation, and Mr. Dzung Nguyen for technical assistance. Finally, I am deeply grateful to my parents and friends for their unending support and inspiration.

## TABLE OF CONTENTS

## LIST OF TABLES

## LIST OF FIGURES

# 1. INTRODUCTION

## 1.1 Goals and Objectives

The purpose of this research is to create electrospun bicomponent polymeric nano-fibrous complexes for various potential applications, such as water treatment, coating, sensors etc. Nanofiber consisting of both natural and synthetic polyelectrolytes may possess unique properties derived from charged polymers and a high specific surface/volume ratio. There has been much research on polyelectrolyte multilayer (PEM) films, demonstrating the feasibility of creating insoluble complexes with a desired surface composition[1]. Electrospinning is a straightforward and versatile technique to fabricate nanofibrous nonwoven mats. The highly porous structure at nano-scale are advantageous to fluid transportation and provide massive sites for binding purposes, which is an ideal candidate for filtration, tissue engineering, etc[2].

The naturally derived polysaccharide, chitosan, is promising for use in biomaterials due to its binding capabilities with lipids and cholesterol, as well as its antibacterial and antifungal properties. Some prominent applications of chitosan include burn/wound dressings and tissue engineering scaffolds[3]. Synthetic polyelectrolytes are also of interest, too. For instance, poly(acrylic acid) PAA, a water soluble polyacid, is frequently employed as a scaffold for immobilization of biologically active molecules or metal ions[4]. It has also been utilized in controlled drug release and as a superporous hydrogel[5].

The existing challenges to electrospinning of chitosan come from to its high solution viscosity and polycationic nature[6]. The stiff backbone due to protonated amine group in

acidic solution results in difficulty in generating nanofibers with controlled characteristics via electrospinning. Readily electrospun, PAA, however, is water soluble. Therefore, pure PAA nanofibers do not retain their structural integrity in water. Fabricated via coaxial electrospinning, bicomponent electrospun nanofibers, which are composed of PAA residing at sheath and chitosan in core, could help increase specific functionality in non-neutral conditions if the two oppositely-charged polyelectrolytes form an insoluble complex[7]. The positively charged chitosan in core would be covered a thin layer of PAA to balance the charges at interface via electrostatic force[8].

The goal of this research is to engineer a polyelectrolyte fibrous structure mentioned above via coaxial electrospinning. The end product with likely core-sheath structure will tend to have a specific composition at surfaces, which is vital important if it is used in medical application. After soaking the electrospun mats in water, the two opposite charged polymers are expected to form insoluble complexes by salt linkages, retaining the overall structure. Therefore, it is of great interest to study the changes, both composition and morphology, of the electrospun mats before and after soaking in water. The surviving structure and its composition will demonstrate effective interfacial interactions between the two polyelectrolytes.

# 2 LITERATURE REVIEW

## 2.1 Importance of Biomaterial Surfaces/Surface area

Although the bulk of a biomaterial governs its overall mechanical and physical properties, the biological responses are more critically related to the surface composition of such materials. Nanofiber surfaces can be further tailored via diverse techniques, such as self-assembly, plasma treatment, chemical modification, and so on. After elaborately designing the material surfaces, the products are endowed with desired end properties *in vivo*. Examples include absorption or release of a specific chemical, providing necessary sites for cell proliferation or attachment or enhancing/inhibiting a metabolic tissue response depending on the specific composition of the material[9].

Kujawa, et al. have studied the structure-properties relationship of the layer-by-layer (LbL) deposited nanofilms composed of chitosan and hyaluronan[1]. The LbL nanofilms are difficult to manipulate for medical purposes and are not ideal for cell attachment and proliferation due to lack of suitable porosity. Producing nanofibers via electrospining is an alternative approach for solving problems of this kind. Nanofibrous mats created by this approach can provide high surface area/volume ratios as well as large amount of porosity, behaving like bioinspired scaffolds[10].

### 2.1.1 Applications of electrospun mat

The characteristic porous structure at nano-scale allows the electrospun mat to be applied to filter, multifunctional membranes[11], wounding dressing and tissue scaffold, etc[12].

Fibers directly electrospun onto the injured skin could form a fibrous dressing, supporting healthy tissue to regenerate without going through tradition formation of scar. Nano-pore sizes also avert bacteria whose width mostly at micro scale from invasion that otherwise may infect the vulnerable wound. High porosity and surface areas, 5–100 $m^2/g$, facilitate fluid transportation and dermal delivery[6].

Mao's group has developed biomimetic environments for cultivating stem cell called the stem cell niche[13]. Six controls include carboxylated, hydroxylated, and aminated surface-functionalized polyethersulfone (PES) nanofiber meshes and PES films had been studied. The results show that both the topography of the matrix and surface biochemical nature of the nanofibers instruct the self-renewal, maintenance and engraftment property of these hematopoietic stem cells (HSCs). Upon altering the above two factors respectively, they are striving to explore effective methodologies for stem cell expansion and differentiation, and commercialize in the field of stem cell-based angiogenesis therapy.

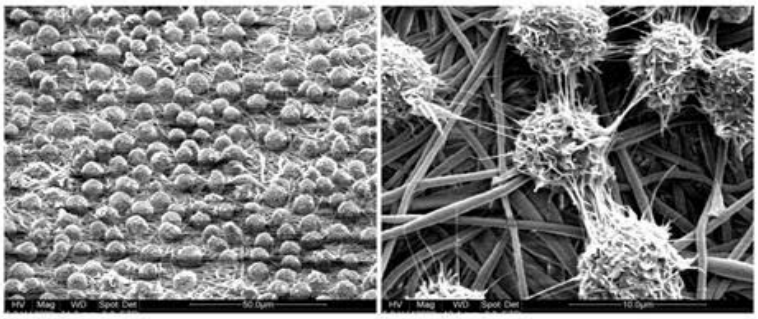

**Figure 2.1:** SEM images of human cord blood hematopoietic stem cells (HSCs) cultured on aminated nanofibers forming circular colonies after 10 days of expansion[13]

## 2.2 Techniques for nanofibrous scaffold fabrication

### 2.2.1 Self-assembly

Self-assembled 3D nanofibrous scaffolds simulate the porosity and gross structure of the natural extracelluar matrix (ECM). One advantage is that fiber diameters derived from this technique commonly range from 5-25 nm. This "bottom up" approach is defined as spontaneous association of molecules under equilibrium conditions into a stable, well-organized structure by non-covalent bond, such as hydrogen bonding, hydrophobic and electrostatic interactions. Although fairly weak and susceptible to disintegrated, these forces manipulate and determine the deployment of these biomacromolecules in the overall structure[14].

This type of fiber is typically consisted of peptide-amphiphile (PA) macromolecule. Manipulated by pH, they spontaneously assemble into a roughly cylindrical configuration via hydrophobic alkyl chain aggregation. Since cells in the these nanofibrous network survived and proliferated well, self-assembled PA system could be used for cell transplantation or other related tissue engineering applications[15].

### 2.2.2 Phase separation

The merit of thermally induced phase separation is the simplicity of creating porous polymer membranes without using any special setups. The porosity and mechanical properties of the scaffold can be controlled by changing parameters, such as solution concentration, gelatination temperature and solvent composition, but it is very difficult to manage the fibrous structure orientation.

When a specific polymer solution undergoes a decrease in temperature, two phases would form, a polymer-rich phase and a polymer-lean phase. Gradually, gelation would occur causing the polymer-rich phase to form a network structure. The spaces originally occupied by the solvent would become pores via extraction like vaporization or sublimation[16]. In Zhao's work, various chitosan acetate structures, including nano-fibrous, microfibrous, film-shape and floccules-like, were generated by varying the aforementioned parameters[17].

### 2.2.3 Template Synthesis

Template synthesis involves utilizing a template to produce nanofibers. A pump was used to forces the polymer solution on through a membrane with cylindrical nanopores arrayed. The extruded solution then enters a coagulated bath, and forms nanofibers. The diameter of the nanofibers depends on the pores in the membrane, and the length can be controlled via altering melt time and temperature. This technique has been used to obtain nanofibrous polymers, metals and semiconductors[18].

### 2.2.4 Electrospinning

Electrospinning has proven to be efficient and relatively straightforward technique to fabricate porous structure at nano scale. It relies on the use of a high voltage source and a grounded collector to create an electric field which promotes the formation of fibers. The spinning solution contained in a syringe or barrel is usually fed by a pump or gas pressure, and then it goes through a conductive needle subjected to the high voltage. The pendent droplet deforms to be followed by an emergence of a tiny cone known as the Taylor cone, from which the polymeric jet will emanate. This occurs because the surface area must increase to accommodate the excess charges reside on the droplet. Due to disruption of the electric field, the thin jet enters a region of whipping instability and is further stretched to tiny fibers at micro-/nano-scale. They eventually are collected on a grounded plate forming a nonwoven mat. So far, many kinds of polymeric nanofibers have been generated using this technique, for instance, polyvinyl alcohol (PVA), polyethylene oxide (PEO), polyurethane (PU), polycaprolactone (PCL), nylon and so on[19].

In order for this process to be successful, variety of parameters have been investigated and are discussed as follows.

#### *2.2.4.1 Processing factors*

Applied voltage, tip-to-collector distance and flow rate are three main processing factors for manipulating the electrospinning process. The former two factors plus solution conductivity primarily control the charges distribution on the pendent droplet. If other parameters are fixed, each system has an optimal applied voltage range. Being out of the

range results in defects in fibers or even failure of jet formation. Tip-to-collector distance, which partly determines electrical field strength, provides space for whipping instability and jet solidification. This leads to fiber diameter decreases with increasing distances from the spinneret. Beaded fibers occur if the distance is too short to give adequate drying for the fiber[20].

Polymer feed rate has influence on fiber morphology as well as mat porosity. It maintains the Taylor cone by keeping a mass balance between the fed solution and ejected one. It has been reported that fiber diameter and pore size increase as flow rate increases until formation of ribbon-like structure[21].

*2.2.4.2 Material parameters*

The basic requirement for fiber formation is sufficient inter-chain entanglements, so polymer concentration, which affects both viscosity and surface tension of the solution, plays a crucial role in electrospinning process. If it is too dilute, the as spun fiber will break up into droplets due to the effects of surface tension, whereas a concentrated solution enables high viscosity making jet initialization extremely difficult. It is reported that as the polymer concentrations increase, the as spun structures change from highly beaded fiber to uniform one, and eventually to a ribbon-like structure[21].

Solvent properties, such as polarity, volatility and miscibility, are also critical to fiber structure and porosity. High vapor pressure solvent may bring about irregular multiple jets emerging from the droplet. As jet travels through the atmosphere, solvent volatility affects phase separation process that determines the structure of the solidified fiber. Megelski, et al.

examined the polystyrene fibers fabricated from mixed solvent systems prepared from various ratios of dimethylformamide (DMF) and tetrahydrofuran (THF). 100% THF as solvent give rise to many deep pores embedded in fibers, whereas smooth fibers yielded from 100% DMF solvent. Between these two extremes, pores gradually became enlarged and shallow as the solvent volatility, THF ratio, decreased[22].

Since most synthetic polymers do not carry a charge, it is preferred to increase solution conductivity by adding extra salts or polyelectrolytes in the solution[23]. Solution with higher conductivity undergoes a greater tensile stretch caused by self-repulsion of the excess charges distributing on the surface. It also prevents axisymmetric instability and creates thinner fibers to some extent[24]. A number of general effects of electrospinning parameters on fiber morphology are shown in Table 2.1.

**Table 2.1:** Effects of electrospinning parameters on fiber morphology[25]

| **Parameter** | **Effect on fiber morphology** |
|---|---|
| Applied voltage ↑ | Fiber diameter ↓(within optimal range) |
| Feed rate ↑ | Fiber diameter ↑ (beaded morphologies occur if the flow rate is too high) |
| Distance between capillary tip and collector ↑ | Fiber diameter ↓((beaded morphologies occur if the distance between the capillary and collector is too short) |
| Polymer concentration (viscosity) ↑ | Fiber diameter ↑ (within optimal range) |
| Solution conductivity ↑ | Fiber diameter ↓ |

## 2.3 Polyelectrolytes and their electrospun nanofibers

Polyeletrolytes are macromolecules which contain a substantial portion of constitutional units bearing ionic or ionizable groups, or both. They can be either synthetic or natural. Examples of the polymeric electrolyte include nucleic acids, some polysaccharides, polyacids, polybases, and their salts etc. Compared with the uncharged polymer solutions, the charged chains coupled with their counter ions behave rather uniquely, particularly in polar solvent. Some features are[8]:

(1) The crossover from dilute to semidilute solution regime occurs at much lower polymer concentrations than that in solutions of neutral chains. (2) The viscosity of polyelectrolyte solutions is proportional to the square root of polymer concentration $\eta \sim c^{1/2}$ (Fuoss' law), while for solutions of uncharged polymers at the same concentration the viscosity is proportional to polymer concentration. (3) Polyelectrolyte chains in semidilute regime follow unentangled dynamics in a much wider concentration range and the crossover to the entangled dynamics occurs further away from the chain overlap concentration than in solutions of uncharged polymers.

### 2.3.1 Natural polymer

Natural biopolymers are of interest, because they simulate a biomemetic environment for tissue regeneration. However, variation in batch quality is inevitable as they are extracted from different sources. Apart from that, the nature of these materials, such as high molecular weight, stiff backbone (typically polysaccharide derivation), is disadvantage to produce submicron or even thinner fibers.

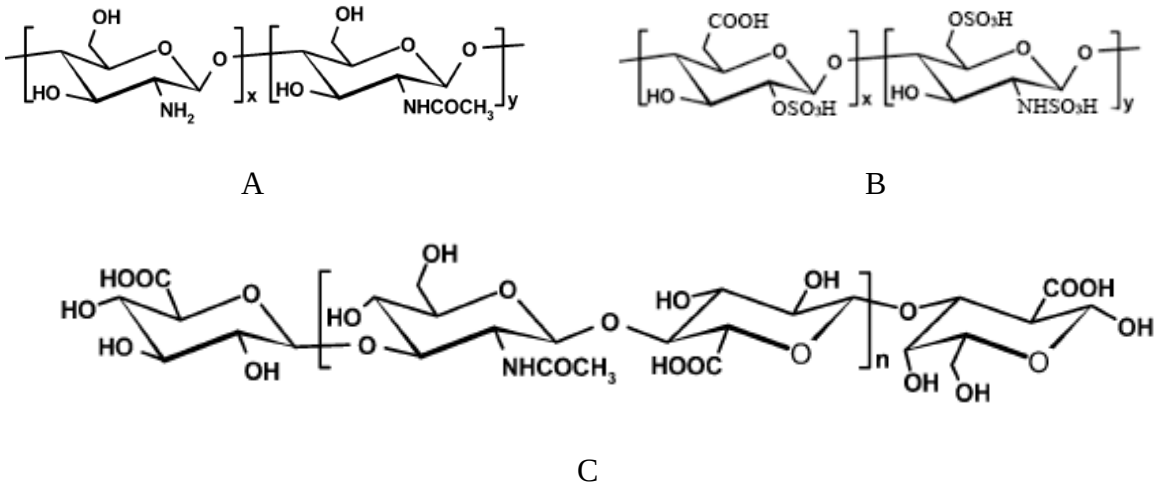


**Figure 2.2:** Chemical structure of (A) chitosan[1]; (B) heparin; (C) hyaluronan[1]

*2.3.1.1 Chitosan*

Chitosan (Figure 2.2 (A)) is nontoxic, biodegradable and antibacterial natural polymers that extensively used in biomedical applications and cosmetics. However, the rigid D-glucosamine structures and high crystallinity lead to poor solubility in conventional organic solvents. Geng, et al. reported electrospun chitosan nanofibers with an average diameter of 130 nm created from concentrated acetic acid (HAc) solution. They suggested that HAc decreases surface tension of chitosan solution and increases the charge density residing on the jet, enhancing fiber extension[26]. Moreover, another group confirmed their results and pointed out that the fiber structures were actually time-dependent. As a thin layer of fibers deposited on the foil within a few minutes, distortion of the electrical field brought about splits and branches on the main trunk[27].

Ohkawa and co-workers made a significant breakthrough, finding that chitosan trifluoroacetic acid (TFA) is more readily electrospun[28]. Indeed, their further work pointed out that with the incorporation of a less volatile solvent, dichloromethane (DCM), the ternary system had a good control of fiber size, and reduced the presence of small beads and branches[29].

Some other work focused on chitosan-containing fibrous composites which were typically blended with poly(ethylene oxide) (PEO) or poly(vinyl alcohol) (PVA)[30][31]. These solutions appeared better electrospinable properties due to the assisting-polymer drive effect. In fact, phase transformation of the ternary system gave rise to a vague core-sheath structure in some cases. Zhang, et al. got this sort of fibers from PEO/CS homogeneous solution, and verified that CS is the major component of the outer layer[32].

*2.3.1.2 Hyaluronan (HA)*

Another commonly used natural polymer in tissue engineering is Hyaluronan, a polysaccharide composed of repeating glucuronic acid and acetylglucosamine (Figure 2.2 (C)). HA aids in cell migration, cell proliferation, angiogenesis, and phagocytosis, healing wounds faster.

Several studies pointed out that high viscosity and surface tension of hyaluronan solution led to failure of electrospinning. Chu and co-works designed an air-blown system close to the spinneret to provide additional shear forces as well as heat, aiming at facilitating solvent evaporation. With the help of such setup known as "electro-blowing", the hyaluronan solution was able to continuously generate nanofibers ranging from 49 to 74 nm[33].

Wang, et al. chose cocamidopropyl betaine, an antibiotic agent, as a surfactant to solve the above problems. Although he fibers electrospun from aqueous solutions appeared inconsistent, the obtained meshes were the best type of wound dressing compared to adhesive bandage, sterilized solid HA, and gauze with Vaseline dressing[34].

*2.3.1.3 Heparin*

Heparin is a highly sulfated glycosaminoglycan (Figure 2.2 (B)). It primarily serves to immobilize growth factors which are critical to simulating cellular activities. So far, no pure heparin nanofiber has been fabricated yet due to its strongly charged backbone.

Viswanathan, et al. have prepared cellulose-heparin fibrous composite from room temperature ionic liquid (RTIL) via electrospinning[35]. The micron-sized fibers fabricated from the nonvolatile system seemed rough and nonuniform, but heparin in the product preserved intact and bioactive.

Casper, et al. found that only trace mount of low molecular weight heparin (LMWH) (0.2wt%) mixed with PEO (8wt%) aqueous solution were able to be electrospun. Under UV detection, the labeled LMWH were found thoroughly distributed in the fibrous mat. Moreover, PLA nanofibrous meshes containing PEG-grafted LMWH were electrospun, and showed better binding property and longer dimensional maintenance than simple LMWH/PLA mixed nanofibrous mat[36].

### 2.3.2 Synthetic Polymers

Synthetic biodegradable polymers could offer many advantages over naturally-derived ones. Normally, they are more easily processed and tailored for desired functional properties, both chemical and physical. The inherent high strength along with great flexibility makes them durable scaffolds for tissues replacement. The main demerit is synthetic polymer can lack biocompatibility to some extent.


A B

**Figure 2.3:** Chemical structure of (A) polyethyleneimine (PEI); (B) poly(acrylic acid) (PAA)[37]

*2.3.2.1 Polyethyleneimine (PEI)*

PEI belongs to polycation that contains high density of primary, secondary, tertiary and/or quaternary amino groups. Though cytotoxic to many cells, it has been widely used in its protonated form as a gene delivery agent. Instead of branched PEI, linear PEI was synthesized from poly(oxazoline) and successfully electrospun from methanol solution. The diameter of the resulted fibers ranged from 200nm to 2μm based on the applied voltage. Crosslinked agents, succinic anhydride and 1,4-butanediol diglycidyl ether, were further employed to form an insoluble network. The post-spin treatment increased the content of

quaternary amino and lowered the overall basicity of the mat. Cell viability suggested that the swelled scaffolds support growth of normal human fibroblasts cells, which may serve as a skin substitution[38].

*2.3.2.2 Poly(acrylic acid) (PAA)*

Poly (acrylic acid) (PAA) is an anionic polyelectrolyte which was frequently used for capture of biologically molecules and metal ions. It is also used to prepare porous hydrogel and fast disintegrating tablet.

The polyacid nanofibers were able to be generated from both aqueous and DMF solutions. Several processing effects, involving solution concentration, applied voltage and conductivity, were studied. Heat capacity test revealed that the mats underwent different process had different amount of water residue, free volume, and capacity of dehydration. To avoid instantaneous dissolution, β-cyclodextrin was mixed in the solution before electrospinning as cross-linking agent. After heat treatment, the resulted mat could survive buffer and appeared strongly pH-responsive swelling behaviors[39].

### 2.3.3 Process of Polyelectrolyte Complex Formation

Nanofiber complexes derived from two weak opposite charged ployelectrolytes were obtained in Rashkov's group via electrospinning[7]. They calculated the ratio of the two different charged polymers in advance to ensure most of the charged groups in one type of polymer are able to find their partners bearing counterions from the other type, and then prepared a homogenous solution using a ternary solvent system to deter premature

polyelectrolyte complex (PEC) formation. If polyelectrolyte complex formation occurs prior to the stretching process, no matter in the form of gel or robust precipitation, fiber generation will fail[40]. This occurs because the solvent is incapable of evaporating properly in a hydrogel or the resulted solid complexes resist further orientation. The electrospun fibrous mat was finally rinsed in de-ionized water to remove the inorganic counterions while the entanglements could maintain the integrity of the mat. This allowed sufficient time for electrostatic force establishment deriving from polymer charge compensation (polymer/polymer ion pairs, intrinsic compensation).

Although polyelectrolyte complexes retain their structure after soaking in water, they are not always stable. One component may lose its charge at acidic or basic pH, accompanied by partial dissociation. Concentrated salts in the external bath force some swelling (extrinsic compensation), and are able to disentangled the complex back to individual chains (shown in Figure 2.4 by the arrow)[41]. To further inhibit disassociation in buffer, normally a thermal treatment was conducted to form covalent bond, like peptide, to replace the salt linkages and hydrogen bonding.

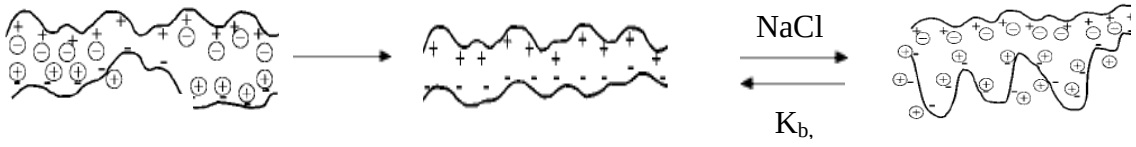


a. Directly extruded fibrous complex
b. De-ionic water washed complex
c. External salt induced swelling

**Figure 2.4:** Polyelectrolyte complex formation[41]

## 2.4 Co-axial Electrospinning for Core-sheath Structures

### 2.4.1 General Set-up and Process

An important method used to form bicomponent continuous nanofibers is to spin two dissimilar polymers within a concentric nozzle, resulting in an end product that comprises the two polymers in a distinct sheath and core form. This technique is referred to as coaxial electrospinning, and has been seen to broad the application of electrospun materials, especially for polymers that is difficult to be spun alone[42]. Coaxial electrospinning improve the properties of a nonwoven fibrous mat, such as creating controlled degradation rates, controlling mechanical properties[43], or serving as a scaffold for tissue engineering where a biocompatible polymer is surrounding a less-biocompatible material[44].

A general coaxial electrospinning setup can be seen in Figure 2.5. Two polymers solutions are held in separated reservoirs (or syringes), and are independently fed through a concentric capillaries in order to form a combined Taylor cone and subsequent continuous fiber. The polymer that is intended to be the core solution is fed using a smaller capillary/needle encapsulated in a larger needle which contains the sheath polymer solution.

The process of co-axial electrospinning is conceptually similar to that of one fluid electrospinning. Subjecting to applied voltage, one of the two fluids is more inclined to become a conical shape, and then sheared the other solution via interfacial contact friction to develop a compound cone followed by a co-axial jet (see 2.4.3 for detail). As long as the process becomes stable, the as-spun fibers undergo bending instability for stretch and solidification, depositing on a grounded collector.

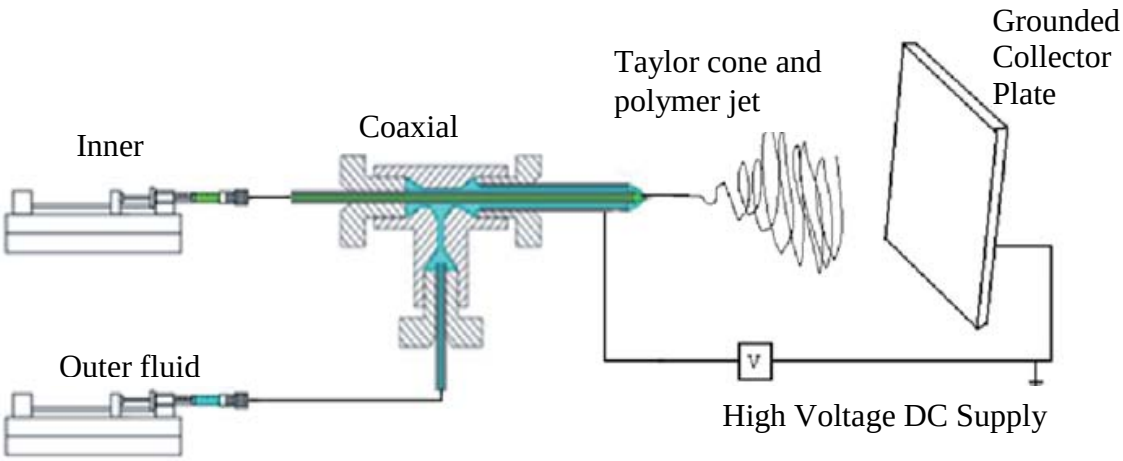


**Figure 2.5:** Typical coaxial electrospinning setup, depicting core and sheath polymers resulting in bicomponent fiber formation

### 2.4.2 Taylor Cone Formation and Electrospraying

Hayati, et al. have quantified the electric force F acting on a unit volume of fluid with the equation

$$F = qE + \frac{1}{2}(\varepsilon - \varepsilon_o)\nabla E^2, \qquad \textbf{Equation 2.1}$$

where q is the charge per unit volume, E is the field strength, ε, $\varepsilon_0$ are the relative permittivity, and the permittivity of free space respectively[45]. The first term on the right side is known as electrophoresis, which is due to the free electric charge and therefore determined by the conductivity of the liquid. Ordinarily, in insulating liquids or an uncharged polymer solution contains very limited amount of ions, a low electrophoretic force for liquid disruption results. Instead the liquid is subjected to the dielectrophoretic force which causes the ions to migrate to the region of highest field intensity, which in the present system is the

tip of the deformed droplet. As a result, a smaller radius of curvature further forms there which could be visualized as a “virtual orifice” through which the jet forms[46]. This can be seen in Figure 2.6:

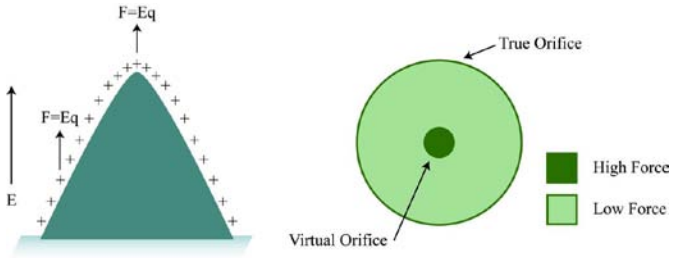


**Figure 2.6:** Taylor cone and electric field gradient force schematics[46]

For polyelectrolytes, which have ionic functionalities, the solution conductivity will be much higher (relative to those of uncharged polymers) and markedly concentration dependent. In this case, electrophoresis dominates the whole process, reducing relaxation time for droplet distortion of the conducting liquid. Charges immediately accumulate at the surface when the voltage is applied. This surface cannot support any tangential electric field and the columbic forces always act perpendicular to the surface, leading to droplet disruption, i.e., electrospraying.

### 2.4.3 Compound cone formation in coaxial electrospinning

In the case of coaxial electrospinning, two mechanisms have been postulated to delineate the spinning process, particularly compound cone formation based on different solution systems.

Moghe, et al. thought electrospinnable sheath was a fundamental requirement to ensure continuously process[42]. A stable Taylor cone created by sheath solution would spontaneously cooperate with core solution by interfacial viscous drag to form a coaxial jet. In case of interfacial slippage, approximate viscosities of both solutions were regarded in favor of the driving process. However, several studies used non-viscoelastic liquids, such as mineral or olive oil, as core material and obtained hollow fibers[47][48]. In fact, electrospinable sheaths working as templates greatly expand inner material selections, either melts or solutions[49].

**Figure 2.7:** Compound Taylor cone[50]

Kurban and co-workers designed a system using electrolyte solution as core solution while non-electrospinable polystyrene (PS)/DMF solution was used as sheath one[51]. Since the outer solution is non-conductive, they pointed out that the charges actually quickly aggregated at the liquid-liquid interface rather than outer surface of the droplet when the voltage applied. Besides, the electrical relaxation time of the inner solution was significantly

shorter than that of the outer one, providing a great impetus for coaxial jet initializing from the interface.

### 2.4.4 Processing parameter

#### *2.4.4.1 Applied voltage*

So far, no work has been done to systemically investigate the effect of applied voltage, because in most studies, only one value of the potential has been reported for a specific process, at which a compound cone stabilized. Below the optimal range, around 1 kV, failure of driving both or any one liquid results in discontinuous dripping. In contrast, above the maximum value may result in separated jets emanating from both sheath and core solutions, and no bicomponent fibers are formed[42].

#### *2.4.4.2 Feed rate*

Feed rate is crucial important to the structure of the bicomponent fiber, especially the thickness of the two layers[21]. Keeping the sheath flow rate constant, several groups found the volume expansion of the overall droplet as core solution throughput increased. Eventually, the sheath solution may fail to appropriately encapsulate the inner liquid causing a disrupted process. Typically, the core feed rate is lower than that of sheath. However, insufficient delivery of core material leads to discontinuous segments embedded in fibers[50].

### 2.4.5 Material parameters

*2.4.5.1 Solution viscosities*

In Moghe's model, the electrospinable sheath solution drove the inner liquid, dominating the fiber formation prcocess. Thus, similar viscosity values are preferred[52]. Several studies showed that jet breakup occurred if the viscosity of the core solution was too low[22]. If the two dissimilar solutions are immiscible, nonviscoelastic core liquid, such as olive oil and brine, is allowed[47].

*2.4.5.2 Solution Concentration*

A similar effect comparing to single fluid electrospinning has been report in co-axial case. Increasing core solution concentration and keeping the sheath one constant, Zhang, et al. found increasing core diameter as well as overall fiber sizes resulted. Meanwhile, the ratio of outer layer thickness to that of inner one decreased[53].

He, et al. inversed Zhang's process by using sheath solutions with different concentrations to create nanofibrous drug release systems. Results showed that fiber diameters increased as the sheath solutions increased[54].

*2.4.5.3 Solution conductivity*

The difference in conductivity between sheath and core solutions has a great impact on charge accumulation, which determines the origin of jet. Yu, et al. found separated jets from both core and sheath solutions might occur if the conductivity of the core solution is high enough. This phenomenon is intensified as the inner solution conductivity became

higher, resulting in discontinuity in formation of core-sheath structure[55]. On the hand, higher sheath conductivity imposes higher shear stress on the inner material, which induced a thinner core structure[21].

*2.4.5.4 Solvent/Solution Miscibility*

If the two solvents used for core and sheath solutions are miscible, mutual diffusion starts as soon as the two fluids encounter at the tip. It might last at the order of 1s before forming a compound cone. Kurban[51] and Li[47] revealed that fiber morphologies strongly depend on degree of miscibility of the two solutions. Fibers electrospun from immiscible solutions had a distinctive core-sheath structure, whereas fibers embedded with dense through-pores were created in semi-miscible systems. Miscible systems failed to form fiber even the sheath solution was electrospinable on its own, because fast diffusion may perturb Taylor cone formation or make sheath material permeate into core solution, disrupting the process.

Sun, et al., however, pointed out that “the characteristic time of diffusion spreading of a boundary” between two miscible solutions was much longer than that spending on whipping instability[56]. Distinguishable core-sheath structure derived from his system demonstrated that extensive mixing did not take place. Additional studies have reported usage of miscible or even same solvent to successfully fabricate core-sheath fibers.

## 2.5 Properties and Applications of Bicomponnet Nanofibers

### 2.5.1 Hollow fiber

Fabrication of nanoscopic and microscopic hollow structures is receiving increasing attention due to their potential applications in microfluidics, catalysis, drug release, etc. Two primary approaches have been adopted.

The first method is based on coating precursor materials on electrospun fibrous template followed by removing the inner fibers via dissolution or thermal degradation. In this way, tube parameters, like inner diameter and wall thickness, are adjustable by altering the template and deposition process respectively[57,58]. In comparison, coaxial electrospinning seems more straightforward and efficient, and has been applied to form different sorts of hollow fibers, inorganic and polymeric.

Li, et al. produced ceramic-based hollow fibers using a mixture composed of a polymer, poly(vinyl pyrrolidone) (PVP), and a ceramic precursor, $Ti(OiPr)_{4,}$ as sheath material[47]. The presence of the highly moisture-sensitive alkoxide was essential to stabilize the coaxial jet and effectively guide the inner oil. Treated with hydrolysis and condensation, the inorganic network enhanced the rigidity of thin walls, and maintained the tubular shape after extraction.

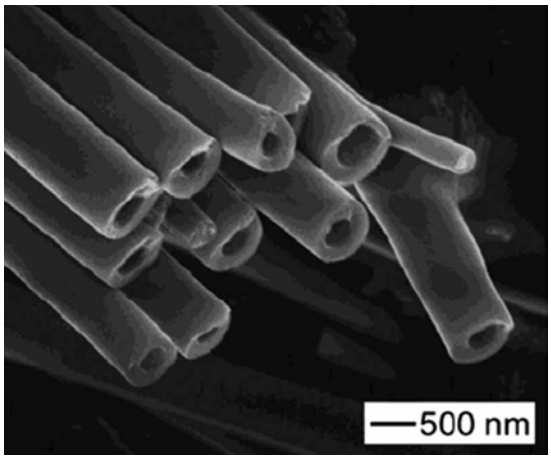


**Figure 2.8:** SEM image of TiO2/PVP hollow fibers prepared by electrospinning[47]

PCL microtubes with an inner diameter of approximately 3μm have been created in Wendorff's group[59]. The process could be considered as a combination of dry/wet electrospinning. The outer surface of the sheath solution experienced a dry spinning process as being exposed to the air, while the inner layer underwent a wet spinning as the inner solute coagulated at the interface. Consequently, the solid film stabilized the interface, and hollow fibers were created.

To expand the applications, scientist further filled these hollow fibers with different substances, such as liquids, biological objects, for diverse purposes.

Jiang, et al. generated PCL nanofibrous released system containing bovine serum albumin (BSA) or lysozyme-doped poly(ethylene glycol) (PEG) as core materials[60]. They found the functionality of the encapsulated substance was not altered after going through the strong electrical field. The releasing rate could be tailored by means of adding PEG, a water soluble macromolecules, in sheath material which created more paths (i.e. through holes) for encapsulated substances release.

Loscertales and co-workers had fabricated hydrophilic nanofibers containing periodic separated bumps in which a hydrophobic liquid was loaded. This structure is attributed to the high interfacial tension which coerced the inner solution breaking up to a finite number of small droplets into the compound cone. The encapsulated droplet eventually recoiled, forming a varicose segments[61].

Some other studies focused on filling with various responsive materials, for instance, phase change materials (PCMs) for energy storage, rhodamine B and fluorescein isothiocyanate (FITC) for multichannel stain, iron-platinum (FePt) for magnetic response. All these inclusions endow the mat with promising novel functionalities[49,62].

### 2.5.2 Bi-component composite nanofibers

Due to phase transformation, one fluid electrospinning is also able to develop core-sheath composites for specific polymer systems. Wei, et al. obtained this type of fibers composed of two incompatible polymers, polyaniline (PANI) and PS, and showed that PS with lower surface tension finally covered the low molecular weight PANI that migrated and aggregated forming inner domain[63]. A similar structure was found in a PEO and chitosan (CS) composite. According to phase diagrams of PEO-CS-$H_2O$ system, the author pointed out that blending ratio, molecular weight of chitosan, and processing temperature were the key factors for the final structure[32]. Since biocompatible chitosan located at the outer layer with adjustable thickness, this product is promising to apply for biomedical fields involving wound care and tissue engineering.

Indeed, coaxial electrospinning viewed as one-step coating may provide unique properties to the products which are hard to achieve by either sheath or core material alone.

Zhuo, et al. fabricated polyurethane-based (PU) shape-memory nonwoven mat. Both core polymer, caprolactone (CL)-co-urethane, and sheath one, pyridine (Py)-co-urethane, were synthesized with specific monomer ratios to ensure the best shape recovery. Under thermal-induced tests, the mechanical properties of the bicomponent fibrous mat behaved very similarly to that of PUPy bulk film, exhibiting high dimension stability and good shape recovery[43].

Zhang, et al. prepared core-sheath nanofibers for the purpose of demonstrating that a biocompatible coating improve cell proliferation[44]. The researchers used collagen, part of natural extracellular matrix, as the sheath, and PCL as core to form the nonwoven mat. Compared to other controls, including pure PCL fibers, a roughly collagen-coated PCL nanofibrous mat prepared by soaking PCL matrix in collagen solution, and two single-component, collagen and PCL, nanofibrous mixture, cell culture revealed the individual collagen-coated fibers created via coaxial eletrospining were most conducive to fibroblast cell migration and proliferation.

### 2.5.3 Fibers from non-eletrospinable material

As mentioned before, electrospinable sheath solution could act as a template to guide the core material into fibrous structure, even if the core solution is incapable of being spun alone. After removing the sheath using a suitable solvent, nanofibers derived from the core

material are obtained. This approach significantly expands the material species for possible nanofiber fabrication.

Using poly(ethylene oxide) (PEO) aqueous solution as sheath solution, chitosan acidic solution was induced to a core-sheath fibrous structure. After dissolving sheath in water, chitosan fibers around 100 nm remained, appearing flatter and more ribbon-like due to swelling (Fig 2.9). FTIR and XRD tests demonstrated that majority of PEO had been removed. However, the obtained chitosan mat was extremely fragile, because the dilute inner chitosan solution for process optimization failed to have sufficient chain entanglements to give satisfied mechanical properties[52].

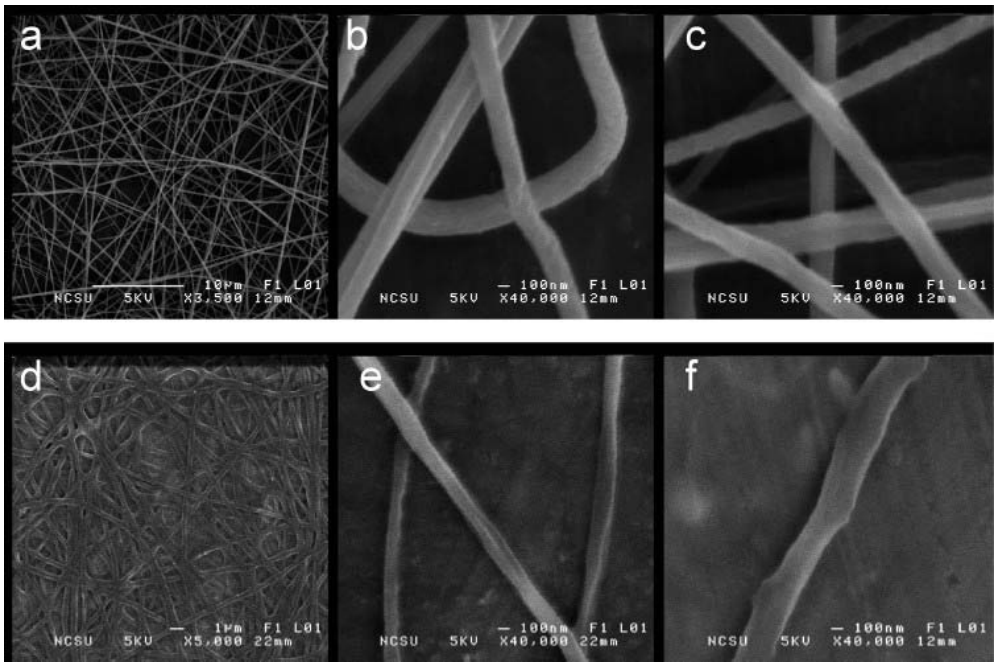


**Figure 2.9**: SEM images of electrospun chitosan-PEO core-sheath nanofibers. (a-c) samples before $H_2O$ rinse and (d-f) samples after $H_2O$ rinse[52]

Yu and co-workers developed a modified coaxial electrospinning process, using a pure solvent as sheath liquid to assist inner solution in forming fiber[64]. They pointed out that N,N-dimethylacetamide (DMAc) with lower vapor pressure prevented rapid loss of core solvent (ethanol), averting gel-like skin or clogging at the spinneret. Because of confining inner solution evaporation and promoting whipping instability, the feed rate of sheath solution has a great impact on the size of the product. Transitions took place if the sheath feed rate was too high, and branched fibers, beaded strings and large joint points in the mat resulted.

In general, coaxial electrospinning is a straightforward and versatile technique to develop hybrid fibers with extraordinaire properties at nano-scale. Some products, which display promising potentials in electronics, composites, tissue engineering etc, stimulate extensive studies in this field. Recent work focuses on designing systems using two dissimilar solutions for desired structures and functionalities as well as investigating the physical interactions between the two solutions in spinning processes. Upon elucidating those parameters, both material and processing, we can have a better command of this nanofiber fabrication technique, and generate higher quality and multi-functional products in near-future.

# 3. EXPERIMENTAL WORK

## 3.1 Materials

All reagents and polymers were used as received.

### 3.1.1 Polymers

Poly(acrylic acid) (PAA), which has a viscosity molecular weight of 450,000 g/mol, was used in the electrospinning experiments. Low molecular weight chitosan (CS) with 75-85% degree of deacetylation has a molecular weight of approximately 50,000-190,000 g/mol based upon viscosity. These two properties of chitosan were verified in the following sections. Both polymers were purchased from Sigma-Aldrich.

### 3.1.2 Solvents

The solvents for preparation of the various solutions include formic acid (FA), 88% (Laboratory) and acetic acid (HAc), glacial 17.4N (USP/FCC/EP/BP). Both were from Fisher Chemical. N, N-Dimethylformamide (DMF), anhydrous, 99.8% and hydrochloric acid (HCl), ACS reagent, 37% were purchased from Sigma-Aldrich.

Hydrochloric acid solution, 0.1N (N/10) (Certified) and sodium hydroxide Solution 0.1N (N/10) (Certified), both obtained from Fisher Chemical, were used in titration.

### 3.1.3 Salt

Sodium acetate anhydrous (fused crystals/certified ACS) was obtained from Fisher Chemical.

## 3.2 Methods

### 3.2.1 Solution preparation

An exact amount of polymer was weighed and put in a plastic container, which was then filled with a predetermined volume of solvent measured by graduate cylinder or pipette. After adding a magnetic stirrer, the container was closed with its own cap. The solutions were stirred for 24 hrs at 300 rpm until a homogeneous solution was formed. The solutions used in the experiments are listed in Table 3.1

**Table 3.1:** Various solution concentrations used for different polymers

| Polymer | Solvent | Concentration % (wt/vol) |
|---|---|---|
| PAA | De-ionized (D.I.) water<br>DMF | 8<br>8 |
| Chitosan (CS) | 90% HAc<br>88% Formic acid (FA)<br><br>1% HCl<br>(700µL 37% HCl + 25mL D.I. water)<br>30% Formic acid | 4<br>4<br><br>4, 4.5, 5, 5.5<br><br>3, 4, 5 |

### 3.2.2 Set-up for single fluid electrospinning

The polymer solution was kept in a 10 mL plastic syringe with a luer-lock connection (Becton, Dickinson and Company (BD)), to which a needle, gauge 20, with luer lock hub (Reusable Type 304 Stainless steel, McMaster-Carr, Atlanta, GA) was attached. The syringe was then fixed onto a programmable syringe pump (NE-1000, New Era Pump Systems, Inc.,

Wantagh, NY), which ensures the dispensing of the solution at a controlled rate. Aluminum foil attached on a round plate was used as a grounded collector for fiber deposition.

The tip of needle pointed to the center of the collector. The distance between the end of the capillary and the collector was kept constant at 20 cm which give acceptable performance. A high voltage power supply (FC Series 120 Watt, Gamma High Voltage Research, Ormond Beach, FL) ,which attached to both the metal capillary and the grounded collector, provided potential difference. The set-up is illustrated in Figure 3.1.

The electrospinning equipment was kept in a fume hood to ensure proper exhaustion of the hazardous solvents.

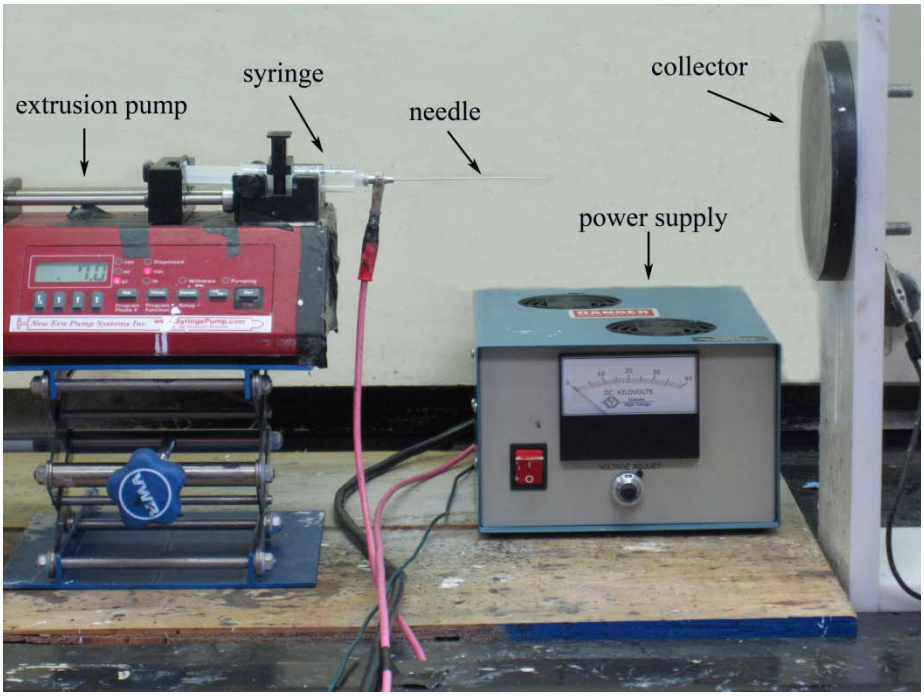


**Figure 3.1:** Single fluid electrospinning setup

**Table 3.2:** Specifications for the capillary needles

| Gauge | OD | ID | Length |
|---|---|---|---|
| 16 | 0.047" | 0.065" | 4" |
| 20 | 0.0235" | 0.0355" | 4" |
| 22 | 0.016" | 0.028" | 4" |

### 3.2.3 Set-up for co-axial electrospinning

A co-axial spinneret system was consisted of a metallic T-connector, one end of which was sealed with a needle having 16 gauge. Another needle with 22 gauge was inserted through the end at the opposite side as well as the bigger needle to give a concentric configuration. The sheath solution was fed through the single-connection end, while the core solution passed through the smaller needle. The set-up is shown in Figure 3.2.

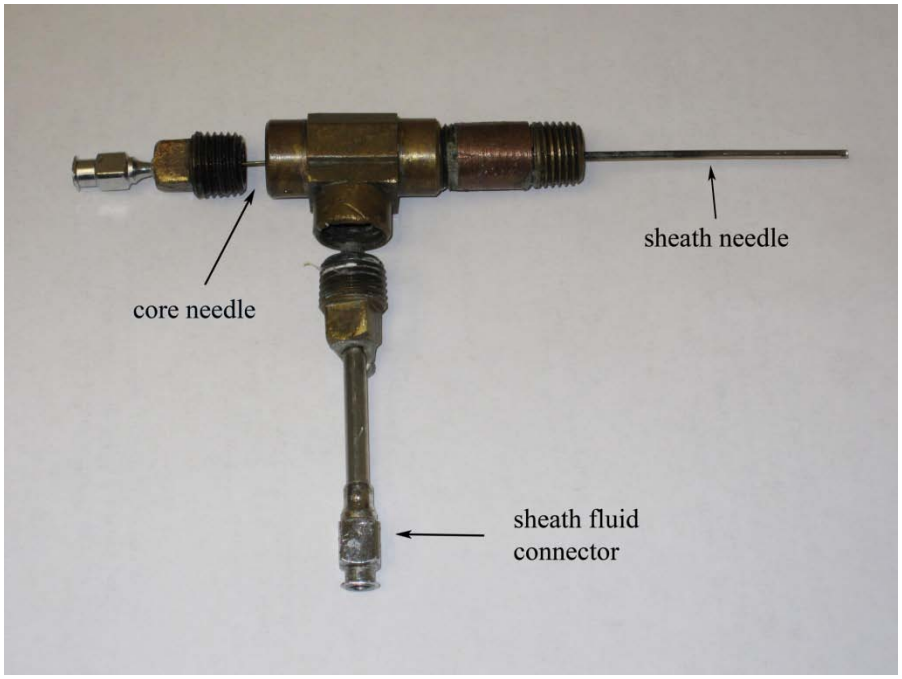


**Figure 3.2:** Coaxial nozzle

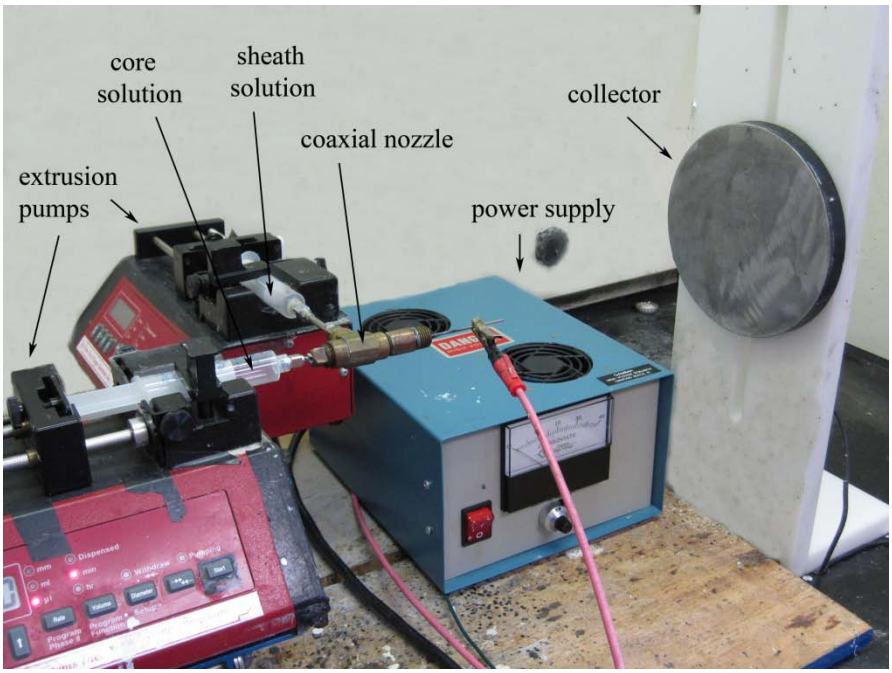


**Figure 3.3:** coaxial electrospinning setup consisting of collector, nozzle, power supply, and two syringe pumps

Two digitally controlled pumps were employed to work separately, which allowed dispensing the two solutions with different feed rates. The rest of the setup was same as that used in one fluid electrospinning. The solution combinations in code for several effective trials are shown in Table 3.3.

**Table 3.3:** Solution codes for effective coaxial electrospinning experiments

| sheath solution (wt/vol) | core solution (wt/vol) | combination code |
|---|---|---|
| 8% PAA in DMF (8PAA/DMF) | 4% chitosan in 30% formic acid (4CS/30FA) | s(8PAA/DMF)c(4CS/30FA) |
| | 5% chitosan in 1% HCl (5CS/dHCl) | s(8PAA/DMF)c(5CS/1HCl) |

### 3.2.4 Sample Preparation

*3.2.4.1 Spinning process*

The major spinning processes are similar in both single and two fluid electrospinning. In the case of one fluid electrospinning, a predetermined value of dispensing rate was set after fixing the syringe onto the pump. Once the polymer solution was consistently flowing out of the orifice, the power supply was switched on. The voltage was adjusted until a jet continuously emanated from the pendant droplet.

In coaxial electrospinning, two syringes containing core and sheath polymer solutions respectively were controlled by two pumps, giving different mass flow rates. In order to examine the effects of material as well as processing parameters on the fiber morphology, various experiments were done by changing polymer solution as well as flow rates. The applied voltages had to be adjusted accordingly to maintain a stable compound Taylor cone. Tip to collector distance was consistently set at 20 cm, which is a compromise between electrical strength and space for jet solidification.

*3.2.4.2 Rinsing of bicomponent fibrous complex*

The bicomponent fibrous mat adhered to the foil was treated in deionized water overnight. The submersion was carried out slowly in case of detachment. After cautiously lifting the foil out of water, the washed mat was dried in ambient conditions for around 48 hours until a constant weight was reached. This aimed at removing the side product derived from complex formation and solvent residue, and to determining the stability of polyelectrolyte-complex nanofibers in aqueous media.

## 3.3 Characterization

Various methods had been employed to characterize samples, including raw materials, prepared solutions, and spun fibers. For chitosan, acid-base conductometric titration and viscosimetry are used to determine its degree of deacetylation (DD) and viscosity average molecular weight, respectively. The zero shear rate viscosities ($\eta_o$) of several solutions were measured by rheometer. Scanning electron microscopy (SEM) was used to examine the electrospun fiber diameters as well as mat morphology.

### 3.3.1 Acid-Base Titration for Determining the Degree of Deacetylation of Chitosan

The degree of deacetylation of chitosan can be determined by the conductometric titration method provided by Khaled and Hudson. First, a known mount of chitosan sample was totally dissolved in quantified 0.1 *N* hydrochloric acid solution. Secondly, as titrated with 0.1 *N* NaOH solution, the conductivities of the chitosan-containing solution change and the corresponding readings were recorded by Orion conductivity cell, model 013030. Finally, the consumed volume of NaOH solution verses conductivity was plotted, in which two deflection points were shown in Figure 3.3.

The first deflection point indicates excess $H^+$ ions, which originated from HCl, have been fully neutralized by added NaOH. The amount of NaOH consuming between the two deflection points, i.e., the width of the trench bottom, corresponds to the neutralization of protonated amino group on chitosan, and can be converted to mole of amino group via Equation 3.1. The solution conductivities eventually sharply increase due to excess NaOH addition[65].

No. of Moles of amino groups $=M_{NaOH}(mol/L)*V(mL)/1000$ **Equation 3.1**

$M_{NaOH}$ is the molarity and $V$ is the difference in the volume between two inflection points.

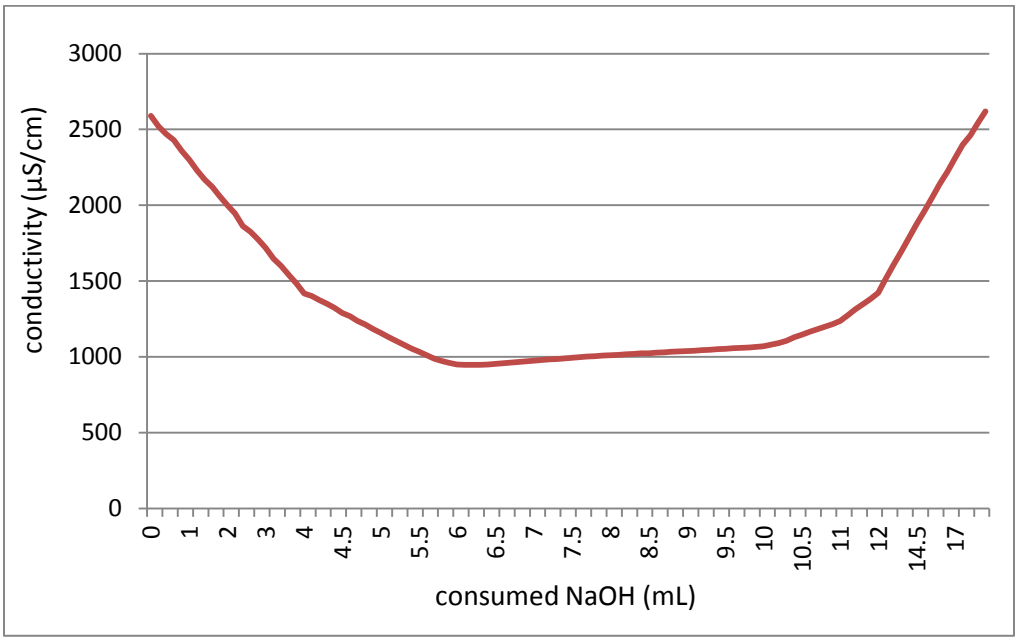


**Figure 3.4:** Conductometric titration curve for chitosan sample.

**Table 3.4.** Degree of deacetylation calculated by conductometric titration method

| Chitason sample | Weight (g) | Mw (g/mol) | Deflection point(mL) Left | Right |
|---|---|---|---|---|
| Commercial | 0.0922 | 161 | 5.9 | 10.0 |
| DD = (0.1*(10-5.9)/1000)/(0.0922/161)*100% = 72% | | | | |

### 3.3.2 Intrinsic Viscosity and Molecular weight determination by Ubbelohde viscometer

The intrinsic viscosity and the viscosity average molecular weight $M_v$ can be determined according to the Mark-Houwink Sakurada equation.

$$[\eta] = kM^{a} \qquad \textbf{Equation 3.2}$$

Considerable research has been done on the viscometric constants, *k* and a for the above equation. Wang and coworkers had found out that the values of viscometric constants change as the DD changes when chitosan was dissolved in an aqueous solution of 0.2M $CH_3COOH$/0.1M $CH_3COONa$.

$$k = 1.64 \times 10^{-30} \times (\%DD)^{14} \qquad \textbf{Equation 3.3}$$

$$a = -1.02 \times 10^{-2} \times (\%DD) + 1.82 \qquad \textbf{Equation 3.4}$$

As the DD increases, more amino groups on the polysaccharide facilitate uncoiling. The expanded dimension eventually increases intrinsic viscosity[66,67].

A series of dilute chitosan solutions were prepared in 0.2M $CH_3COOH$/0.1M $CH_3COONa$ aqueous solution. Cannon-Ubbelohde semi-micro viscometer (size 75 J- 134) carrying a load of each solution was immersed in a water bath maintaining at 30°C. For each concentration, ten effluent times were recorded and averaged. These readings were then converted to relative viscosity ($\eta_{rel}$) and specific viscosity ($\eta_{sp}$) using the Equations 3.5 and 3.6, respectively.

$$\eta_{rel} = t_{solution} / t_{solvent} \qquad \textbf{Equation 3.5}$$

$$\eta_{sp} = ( t_{solution} / t_{solvent} ) - 1 \qquad \textbf{Equation 3.6}$$

in which $t_{solution}$ and $t_{solvent}$ are the time that the polymer solution and pure solvent flow through a specific volume in viscometer. These results are recorded and calculated in Table 3.5

**Table 3.5:** Scheme of intrinsic viscosity measurement of commercial chitosan (DD72%).

| **c (g/mL)** | 0 (solvent) | 0.002 | 0.0015 | 0.001 | 0.0007 |
|---|---|---|---|---|---|
| **Time (sec)** | 101 | 227 | 192 | 186 | 138 |
| **$\eta_{sp}$** | | 1.247 | 0.901 | 0.543 | 0.366 |
| **$\eta_{sp}/c$** | | 623.5 | 600.6 | 542.9 | 522.9 |
| **$\eta_{rel}$** | | 2.247 | 1.901 | 1.543 | 1.366 |
| **ln $\eta_{rel}/c$** | | 404.8 | 428.2 | 433.7 | 445.6 |

A graph of $\eta_{sp}/c$ versus $c$ and $\ln(\eta_{rel})$ versus $c$ was then plotted based on Huggins's equation, and Kraemer's equation, respectively (see Figure 4.4), where $c$ is the concentration of chitosan solution. For predicting the intrinsic viscosity [η], the points were extrapolated to zero concentration, that is the intercept of Huggins's equation. Then the average viscosity molecular weight was calculated based on [η], $k$ and a via Mark-Houwink-Sakurada equation. Several properties of original chitosan are listed in Table 3.6.

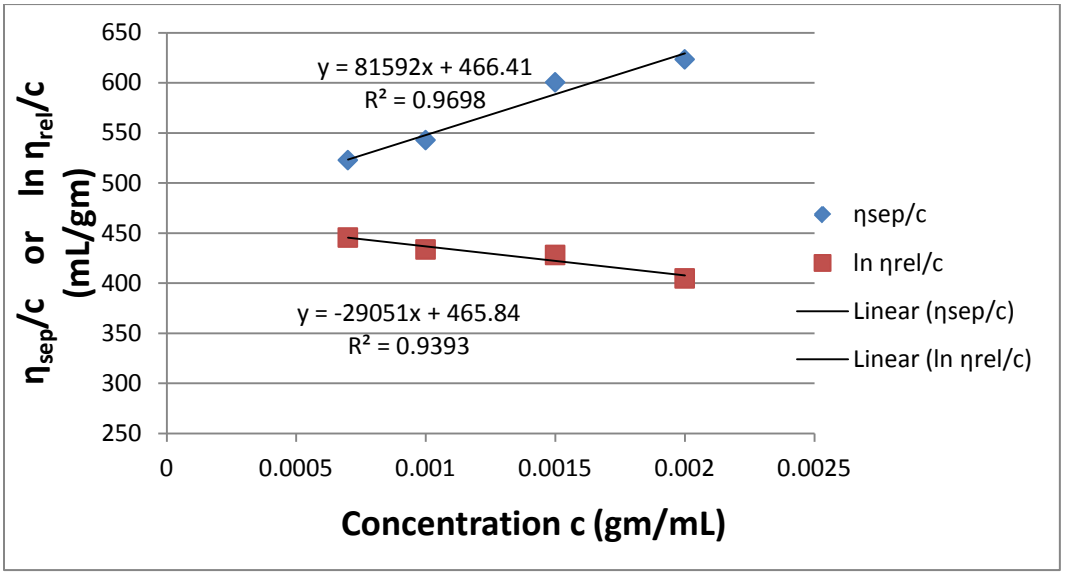


**Figure 3.5:** Huggin's and Kraemer plot of $\eta_{sp}/c$ versus c and ln $\eta_{rel}/c$ versus c for the medium viscosity chitosan in 0.2M $CH_3COOH$/0.1M $CH_3COONa$ aqueous solution.

**Table 3.6:** Properties of commercial chitosan

| Chitosan sample | DD (%) | *k* (mL/g) | a | Intrinsic viscosity [η] | Viscosity average molecular weight, $M_v$ |
|---|---|---|---|---|---|
| commercial | 72 | $1.64 \times 10^{-30} \times (72)^{14} = 1.65 \times 10^{-4}$ | $-1.02 \times 10^{-2} \times 72 + 1.82 = 1.09$ | 466.1 | $8.3 \times 10^{5}$ |

### 3.3.3 Solution pH measurement

pH values of those aforementioned solutions were measured by pH paper (Micro Essential Lab. Brooklyn, NY). Hydrion S/R dispenser 1.0-2.5 was used for acidic chitosan solutions. Results were used to predict and explain premature gel formation which is undesirable for coaxial electrospinning.

### 3.3.4 Rheological Measurement of Solutions

Polymer rheology can be defined as the study of polymer solution/melt under flow and deformation. If a single value of viscosity fails to quantify this behavior, rheometer can replace viscometer offering more parameters to be set and measured. The parallel plate (or plate-plate) system, one kind of shear rheometers, was used in our experiment. It requires a small sample volume, and has the advantage of being able to take pre-formed sample discs which can be especially useful when working with polymers.

An Stresstech HR rheometer (ATS RheoSystems, Bordentown, NJ) is used to measure zero shear rate viscosity. After mounting the sample onto the bottom plate, the 50 mm top plate is calibrated to a 0.400 mm gap. Keeping at 25°C, the sample's viscosity was

measured as a function of stress and/or shear rate. The zero shear rate viscosity ($\eta_0$) was an average of the values in Newtonian plateau region obtained from Rheologica Rheo-Explorer 5.0 software.

### 3.3.5. Scanning Electron Microscopy (SEM)

Nanofibers samples, collected on aluminum foil, were sputter coated by a K-550X sputter coater with Au/Pd having thickness of 100 Å to assist charge dissipation.

Two types of SEM were used: JEOL 6400F Field Emission SEM (JEOL USA, Inc., Peabody, MA) and Phenom$^{TM}$ (Phenom-World B.V., The Netherlands). After coating, the samples were mounted on the SEM and focused, and viewed at magnification between 5000-40,000 times over their original sizes. Those images were the used to evaluate the fiber diameter and consistency.

For images obtained from FEI Phenom, ImageJ was used to measure the diameter of fibers. Firstly the scale was set based on the scaling bar on the SEM image, and then the line length function could figure out the fiber diameter. Averagely 30 fibers were measured in each SEM images.

### 3.3.6 Freeze fracturing

This technique was used to confirm the presence of the core-sheath structure in co-axially electrospun fibers. The fiber mats were immersed in liquid nitrogen for instant freezing. While still in the liquid nitrogen bath, the specimens were poked at various places using sharp tweezers to fracture the fibers. This was done to induce differential fibrillation

between the sheath and the core. The fractured specimens were then viewed under SEM as described earlier.

### 3.3.7 Microtomy

Ultramicrotome (UC7 Cryo, Leica, Wetzlar, Germany) was employed to prepare thin slices (20 nm – 2.5 μm) of samples mounted on the copper grid for TEM characterization. Operated at room temperature, the instrument run according to the program we set, including resin and sectioning with glass knife.

### 3.3.8 Transmission Electron Microscopy (TEM)

Transmission electron microscopy (2000FX, JEOL USA, Inc., Peabody, MA) was used to observe the longitudinal as well as the cross-sectional structure of the electrospun fibers for indentifying the likely core-sheath structure. All samples were run at 80 kV, minimizing the potential damage to the polymeric products.

### 3.3.9 Fourier Transform Infrared Spectroscopy (FTIR)

Fourier Transform Infrared Spectroscopy (FTIR, Nicolet 510P, Thermo Electron Scientific Instruments LLC, Madison, WI) was performed in transmittance mode. The FTIR chamber was purged with dry air to eliminate water vapor.

The data was collected in Attenuated Total Reflectance (ATR) mode using a Germanium tip that directly contacted the sample, instead of using potassium bromide (KBr) powders mixed with the sample. The spectra were observed between 4000 – 700 $cm^{-1}$, with

64 scans having a resolution of 4 $cm^{-1}$. FTIR of pure chitosan, pure PAA and chitosan-PAA core-sheath nanofibers (before and after washing) were performed in order to characterize the surface composition.

# 4. RESULTS AND DISCUSSION

## 4.1 Preliminary Results

In order to verify that the horizontal electrospinning setup which our team built was capable of electrospinning, poly(acrylic acid) (PAA) controls in different solvents were characterized and electrospun. The data derived from solutions as well as spun fibers coincide with published results, which confirm the system meet the demand for further experiments.

Dissolved in dimethylformamide (DMF) and de-ionized water (D.I. water), the two PAA solutions behave quite differently. In aqueous solution, the acid groups of PAA are more likely to disassociate, resulting in a solution conductivity two orders of magnitude higher as compared to PAA/DMF solution (Table 4.1). With respect to viscosity, however, DMF acting as a better solvent forms a bigger solvating envelope, increasing the effective volume of polymer segment and the volume fraction of the polymer coil, leading to higher viscosity.

Furthermore, the two properties have great impact on electrospinning processes. Under similar processing conditions (Table 4.2), discontinuous jets were observed with naked eye emanating from aqueous solution. This may mainly attribute to the low viscosity of the solution that cannot constantly sustain the driving force, breaking into intermittent spinning processes. In contrast, DMF solution was spun with single jet consistently.

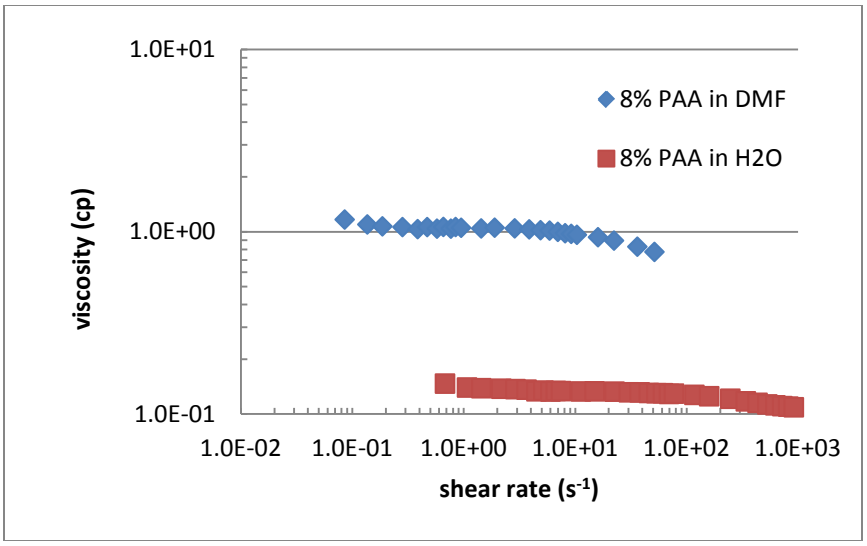


**Figure 4.1:** Viscosity versus shear rate of 8wt% PAA in different solvents.

**Table 4.1:** Properties of PAA solutions

| Polymer | Solvent | Concentration % (wt/vol) | Solution | |
|---|---|---|---|---|
| | | | Viscosity ($\eta_o$) (Pa·s) | conductivity (mS/cm) |
| PAA | DMF | 8 | 1.04 | 0.252 |
| | $H_2O$ | 8 | 0.134 | 97.8 |

**Table 4.2:** Electrospinning Conditions for PAA

| Solvent | Concentration (wt%) | Feed rate (μL/min) | Applied Voltage (kV) | Tip to collector distance (cm) |
|---|---|---|---|---|
| DMF | 8 | 10 | 13 | 15 |
| $H_2O$ | 8 | 10 | 10 | 15 |

The fibers generated from aqueous solution appeared more homogenous in sizes than those from DMF solutions. In addition, they were more loosely packed, giving lager pores (Figures 4.2 A). The higher conductivity of the aqueous PAA solution shorten the time required for the excess charge, in the form of disassociated ions, to move in response to the electrical field enabling greater tensile stretch. Lower viscosity also decreases the bending

rigidity of the jet. These two factors enhance whipping and lead to more uniform fiber[24]. Larger pore size might be caused by the multiple jets, giving rise to more random fiber deposition.

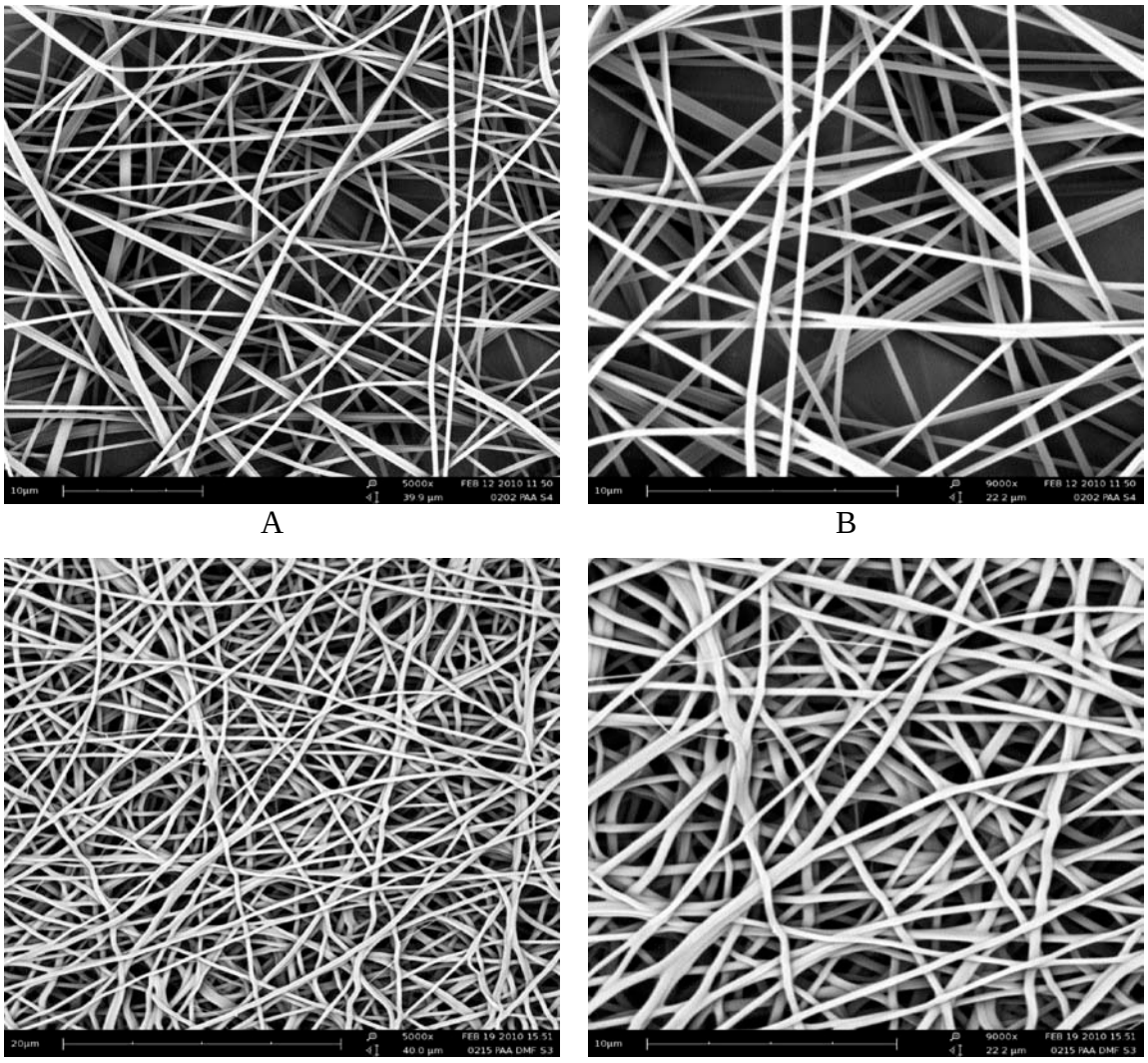


**Figure 4.2:** SEM images of PAA nanofiber generated from aqueous solution A*(5,000x)*, B*(9,000x)* and DMF solution C*(5,000x)*, D*(9,000x)* Spinning conditions see Table 4.2

## 4.2 Coaxial Electrospinning of Bicomponent Complexes

### 4.2.1 Effect of Interfacial Interactions

Although chitosan is more biocompatible than PAA, only a few studies have succeeded electrospinning of pure chitosan solutions. The highly volatile solvents used in those studies were disadvantageous to create compound Taylor cones and stabilize the process.

Therefore, PAA/DMF solution was first used as sheath solution while chitosan was used as core material to investigate the feasibility of fabricating insoluble fibrous complexes. Two solutions, 4 wt% chitosan in 90% aqueous acetic acid (90HAc) as well as in 90% aqueous formic acid (90FA), were used as first trials.

In the case of chitosan dissolved in concentrated acetic acid, a gel immediately formed at the solutions interface. Elasticity of the gel resisted permanent droplet deformation, and no jet occurred.

Since DMF is disadvantageous to PAA disassociation revealed by the low conductivity (Table 4.1), most carboxylic groups still remain in non-ionized form, while most of chitosan amine groups ionize to $NH_3^+$ in 90HAc, which suggests the following complex formation mechanism[68]:

$$\underset{\text{Chitosan}}{NH_3^+} + \underset{\text{PAA}}{COOH} \rightarrow \underset{\text{Complex}}{NH_3^{+-}COOH} + H^+$$

**Figure 4.3:** Mechanism of complex formation

Thus, highly acidic conditions, pH lower than 3[7], are required to inhibit the above reaction. Under those conditions, the carboxylic groups of PAA do not have sufficient charge density to participate in polyeletrolyte complex (PEC) formation with the fully protonated amino group of chitosan[68].

When 4 wt% chitosan in 90FA was prepared and used as core solution, no gelation was observed. However, fast interfacial diffusion in the semi-miscible system results in difficulty in creating a Taylor cone and maintaining the process[51]. Particularly, FA, which is a nonsolvent to PAA and possesses higher vapor pressure than that of DMF (Table 4.4), disrupting the electrospinable sheath (Figure 4.4)[21].

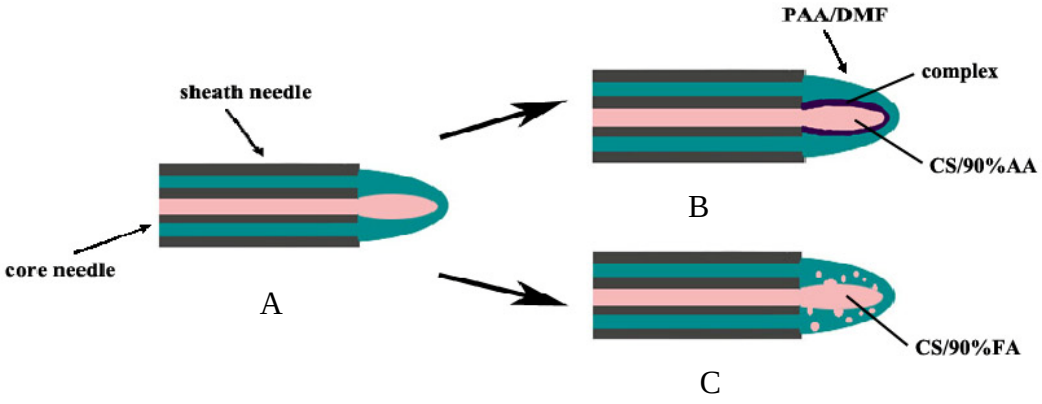


**Figure 4.4:** Schematic of interfacial reaction (B) or diffusion (C)

**Table 4.3:** pH values of prepared solutions

| solution | pH |
|---|---|
| 8 wt% PAA in DMF | 5.48*[39] |
| 4% chitosan in 90% HAc | 2.5 |
| 4% chitosan in 90% FA | 1 |
| 4-5% chitosan in 1% HCl | 1 |
| 3-5% chitosan in 30% FA | 1.5 |

**Table 4.4:** Solvent parameters used for solvent selection for electrospinning[51]

| solvent | electrical conductivity at room temperature (mS/cm) | boiling point(°C) | enthalpy of vaporization (kJ/mol) (1atm at boiling point) | vapor pressure at 20 °C (atm) |
|---|---|---|---|---|
| water | $4 \times 10^{-5}$*[76] | 100 | 40 .8 | $2.75 \times 10^{-2}$ |
| DMF | $6.0 \times 10^{-5}$ | 153 | 47 .6 | $2.24 \times 10^{-2}$ |
| formic acid | 5.5 | 100 | 23. 1 | $1.31 \times 10^{-1}$ |
| acetic acid | $1.12 \times 10^{-5}$ | 118.1 | 23.7 | $1.50 \times 10^{-2}$ |
| HCl[69] | | -85.1 | 16.2 | 42.1 |

### 4.2.2 Effect of Solvent Volatility

In order to solve the problems confronted in the previous series, both dilute hydrochloric acid (dHCl) (1%) and 30% aqueous formic acid (30FA) were used, respectively. Different concentrations of both solutions were prepared to match the viscosity to sheath solution viscosity (Figure 4.5). All of their pH values were tested in advance in case of undesired reactions. It showed that the solvent nature dominated acidity. The pH of the solutions prepared by diluting a strong acid, HCl, are less than 1 no matter the small solute concentration differences, whereas 30% formic acid solutions are around 1.5 (Table 4.3).

We chose 4 wt% chitosan in 30FA and 5wt % chitosan in dilute HCl as core solutions for further trials. Considering the pedant droplet configuration resulted from core and sheath feed ratio, as well as total extrusion rate, we set the processing parameters to those in Table 4.5, in which voltages were cautiously adjusted to stabilize the compound cone.

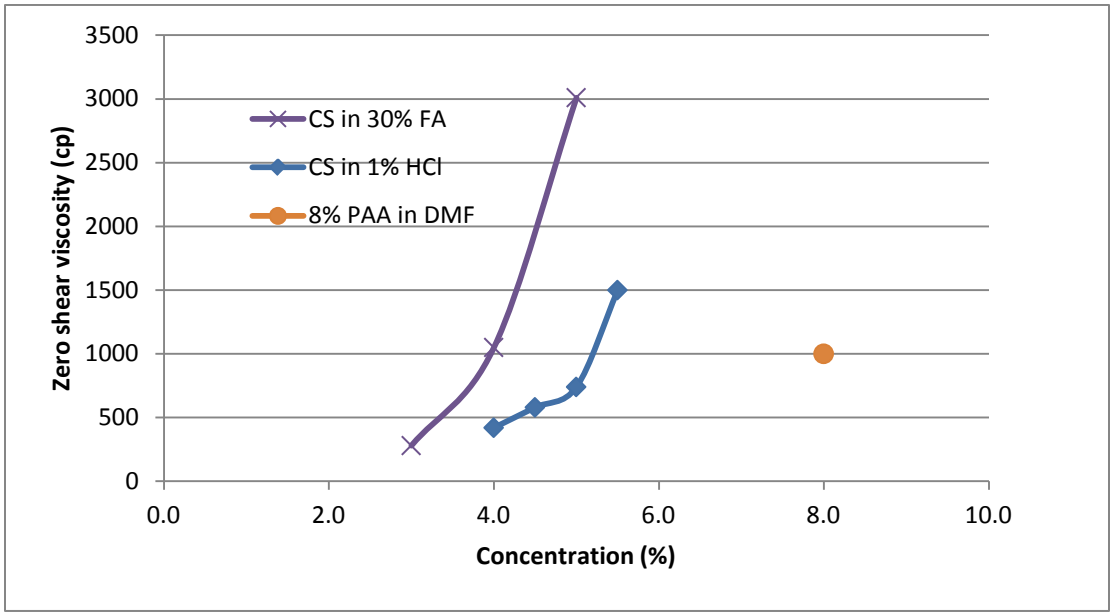


**Figure 4.5:** Zero shear viscosity versus shear rate of chitosan solutions both formic acid and HCl and 8% PAA in DMF

**Table 4.5:** Electrospinning conditions for bicomponent fibers

| Solution systems | Flow rate (µL/min) Core | sheath | Applied voltage (kV) | Tip to collector distance (TCD) (cm) |
|---|---|---|---|---|
| s(8PAA/DMF)c(4CS/30FA) | 6 | 10 | 23 | 20 |
| s(8PAA/DMF)c(5CS/dHCl) | | | 20 | |

Gel formation had not taken place in both trials due to the involvement of plenty of $H^+$ in the core solution, inhibiting reaction illustrated in Figure 4.3.

Using same sheath solution as well as similar processing parameters (Table 4.5), core solutions give rise to major differences in the two products (Figures 4.6 and 4.7). For nanofibers generated from 30% aqueous formic acid as core solvent, SEM images revealed that this solvent is able to evaporate effectively, and most produced fibers are distinguishable. Fibers deposited at the center fused a little, ranging from 244 ± 101 nm, whereas the average size of fibers at the edge was 179 ± 31 nm which appeared more uniform. In contrast, Image A in Figure 4.7 shows a fibrous, yet film-like structure. This is a result of using dilute HCl instead of the 30FA as core solvent, which decreased vapor pressure and increased enthalpy of vaporization of the HCl solvent system (Table 4.4). Wet fibers interlaced on the collector and fused together.

Comparing the Images A and B in both cases (Figure 4.6 and 4.7), we found that fibers located at different areas display different morphologies. Fibers found at the edge of the collector (Figure 4.6 B) look more consistent than those at center (Figure 4.6 A). This may depend on the complex paths that different fibers underwent. Bigger spiral motions within a lager envelope cone are expected for fibers deposited at the edge, in which higher order bending instabilities in the loop actually dramatically increased the traveling distance before fiber reaching the collector[24]. The longer deposition paths support fibers at the edge to stretch, and facilitate solvent evaporation.

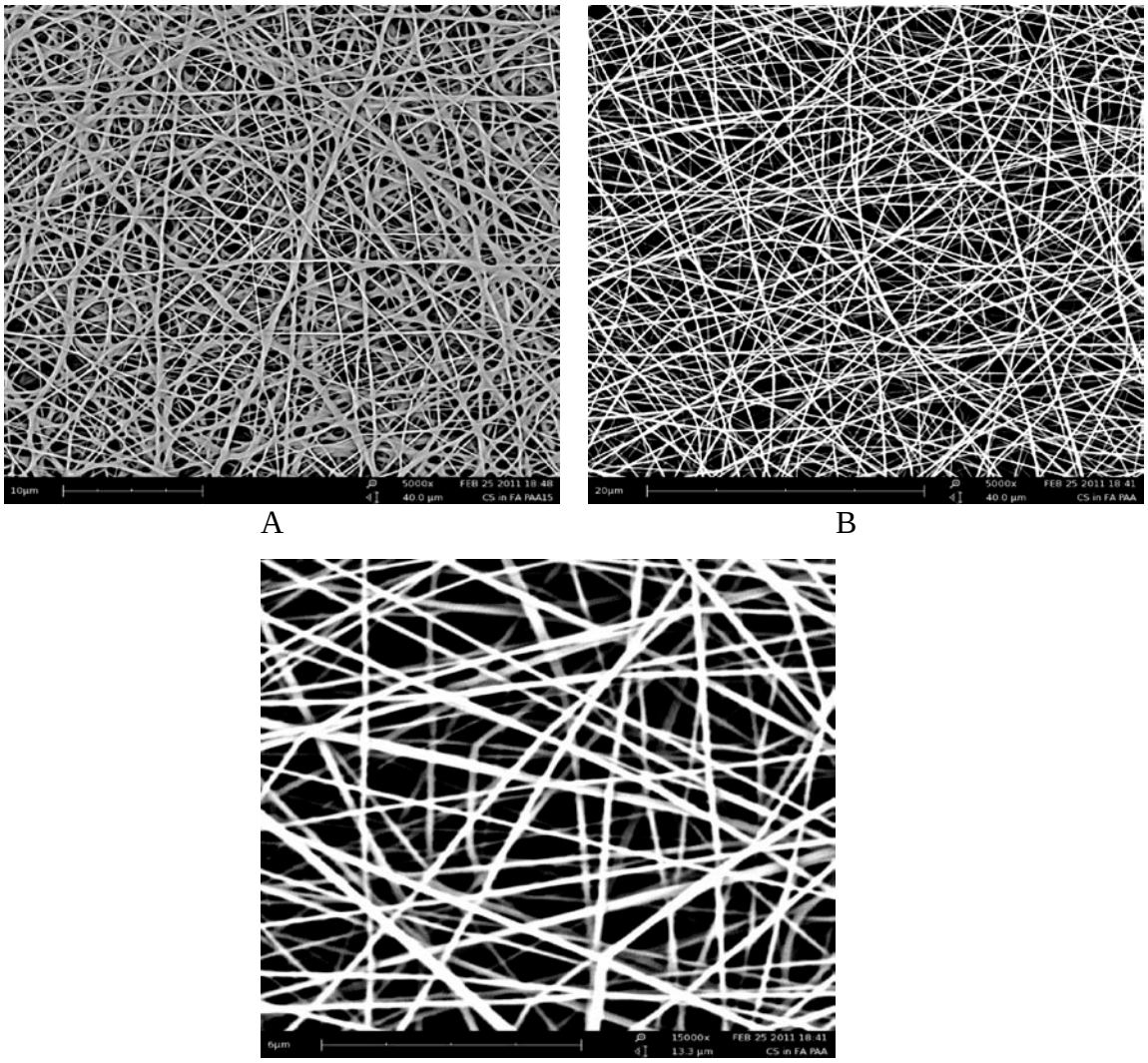


A B

C

**Figure 4.6:** SEM images of bicomponent fibers generated from s(8PAA/DMF)c(4CS/30FA)
A (center of mat, *5,000x)*, B, C (edge of mat, *5,000x, 10,000x respectively)*
Spinning conditions see Table 4.5

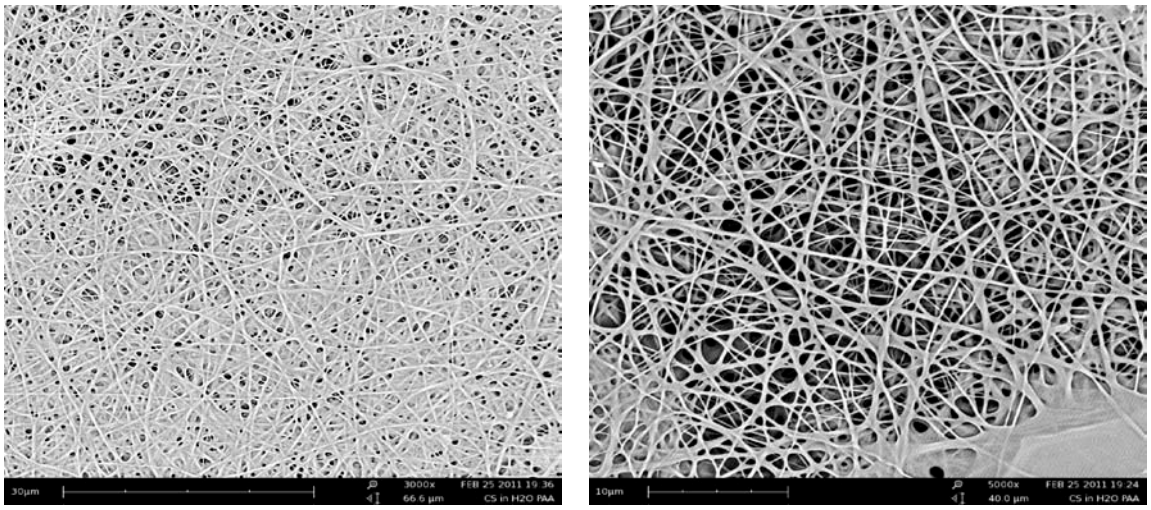


A

B

**Figure 4.7:** SEM images of biocomponent fibers generated from s(8PAA/DMF)c(5CS/dHCl) A(center of mat, *3,000x*), B(edge of mat, *5,000x*)
Spinning conditions see Table 4.5

## 4.3 Complexes after rinsing

The next step is soaking the two fibrous mats, one form s(8PAA/DMF)c(4CS/30FA) and the other from s(8PAA/DMF)c(5CS/dHCl) system, in D.I. water overnight for the purpose of studying of the stability of the fibrous mats in aqueous media. Both white electrospun mats swelled, showing white complexes attached to the foil with another layer of transparent hydrogel atop the complexes.

After cautiously lifting the two mats out of water, the two mats were dried under ambient condition until a constant weight was reached. Both of them appeared dry and opaque to the naked eye. However, SEM revealed dramatic differences in the microstructure of the mats.

For the complex derived from dilute HCl as core solvent, SEM showed that parts of the residue are solid films, while other regions still maintain a nanoscale structure that remained from the original fibers. In addition, large beaks are observed (Figure 4.8). The surviving structures are expected to be made up of chitosan, which is insoluble, and likely PAA residue because of PAA-chitosan complex formation via electrostatic force at the interface. FTIR was later performed to determine its chemical composition.

Several possible factors give rise to the co-existence of the two structures. The residual PAA is capable of swelling tens of times in water[5]. This volume expansion made inter-fiber PAA macromolecules entangle, forming solid films (Figure 4.7 A). While in some other regions, especially near the edge of the mat, porous matrix was found (Figures 4.8 C and 4.9), probably because of the lower density of fibers in that area (Figure 4.6 B). Pores among the fibers was too large to be entirely sealed by the swollen PAA.

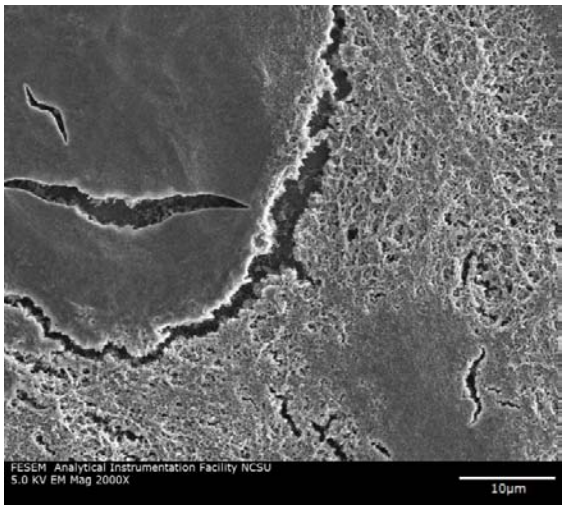


A

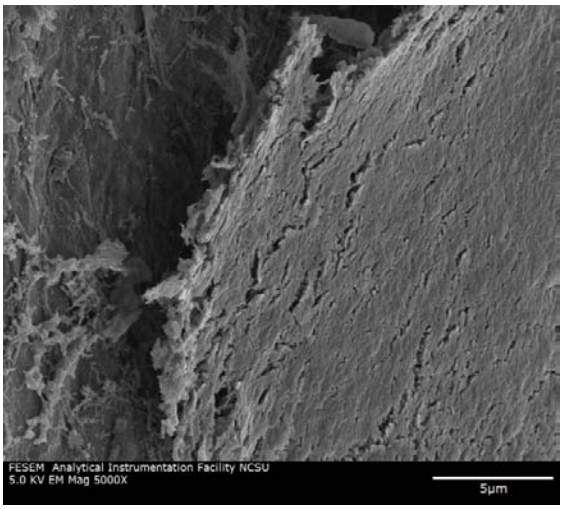


B

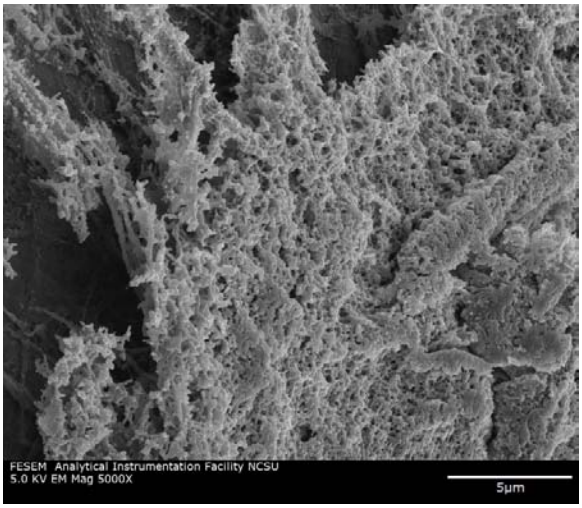


C

**Figure 4.8:** SEM images of polyelectrolyte complex derived from s(8PAA/DMF)c(5CS/dHCl)
A(*2000x*), B(center of mat, *5,000x*), C(edge of mat, *5,000x*)

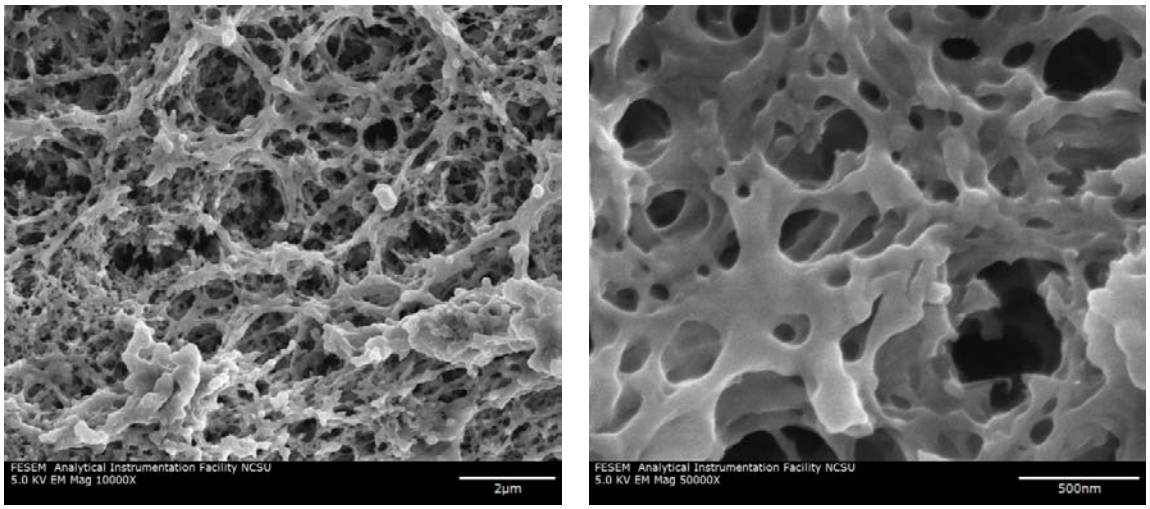


A B

**Figure 4.9:** SEM images of polyelectrolyte complex derived from s(8PAA/DMF)c(5CS/dHCl) higher magnification of Image C in Figure 4.8 A, B (edge of mat, *10,000x, 50,000x respectively*)

For the case using 30FA as core solvent, the overall complex after soaking shows a relatively consistent and regular structure. Although some fibers fused to a sheet, most fibers are still distinguishable and are covered with nano-sized beads (Figure 4.10).

Instead of appearing as a smooth cylinder shape, the coarse topography on the surface may due to mutual diffusion[56, 51], in which both chitosan and PAA solutions might be engaged. Indeed, a previous study revealed that PAA could also diffused into solid chitosan to some extent in the process of soaking[70]. In fact, the surface roughness significantly increase surface/volume ratio.

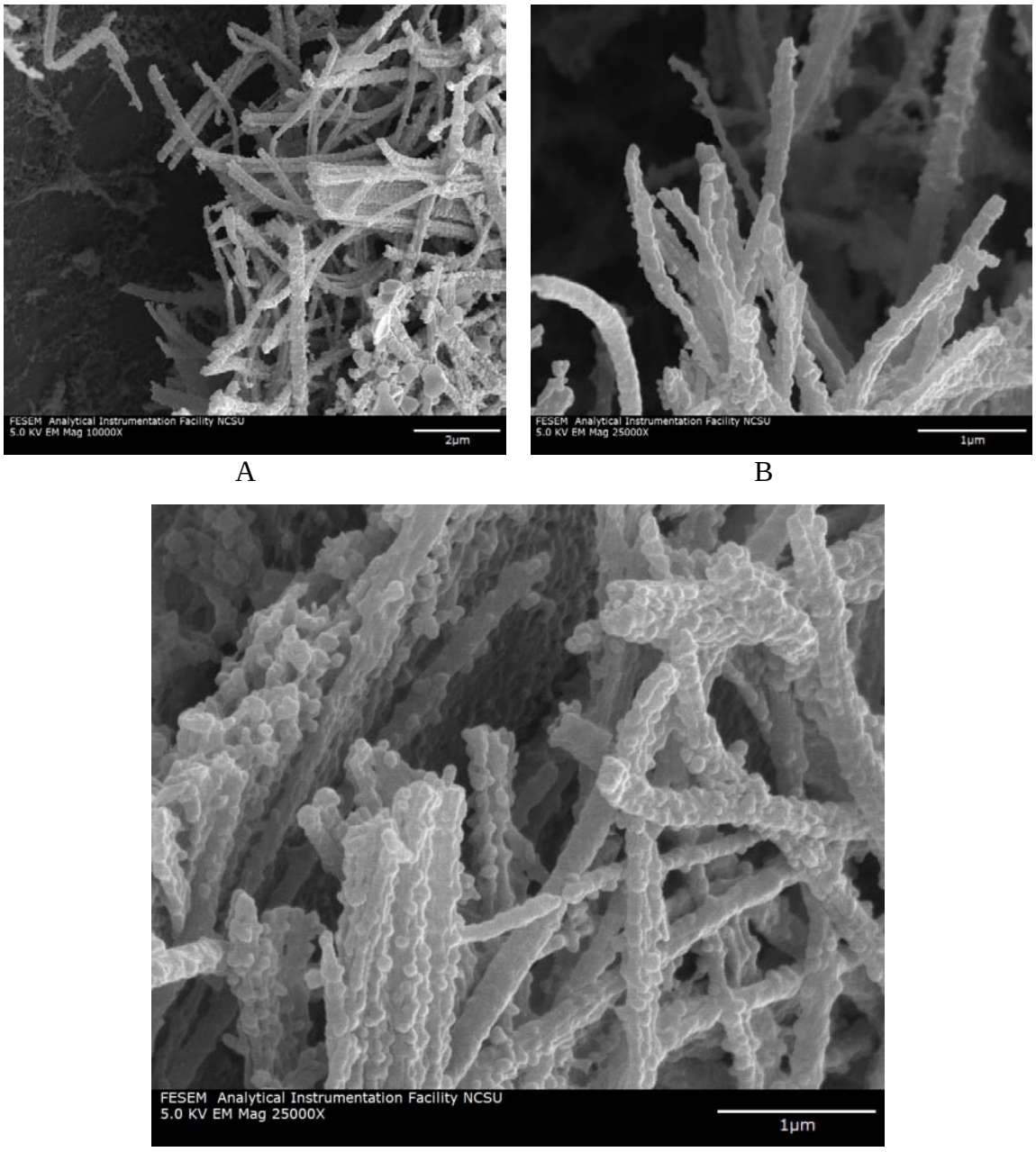


A B

**C**

**Figure 4.10:** SEM images of polyelectrolyte complex derived from s(8PAA/DMF)c(4CS/30FA)

A, B, C (*10,000x, 25,000x, 25,000x, respectively*)

## 4.4 Freeze Fracture

In order to observe the core-sheath structure, as well as possible interfacial regions of the electrospun fibers, we adopted freeze fracture techniques to observe the cross sections of the fibers. Treated with liquid nitrogen, the frozen mats were quickly poked with sharp blade.

As shown in Figure 4.11, the stacked layers delaminated and the electrospun fibers ruptured. This may imply the fiber deposition mechanism in electrospinning when a grounded plate was used as collector. As fiber deposited, regions where electrospun fibers cover the plate are less conductive, so it is harder for the new fibers to dissipate their charge, i.e., become grounded. Guided by the stronger electrical strength originated from the pores[27], the charged fibers are more inclined to deposit on the places where have less pre-existing fibers. Thus, as one layer of fiber paves the collector resulting in a relative even potential area on the collector, the second layer continues.

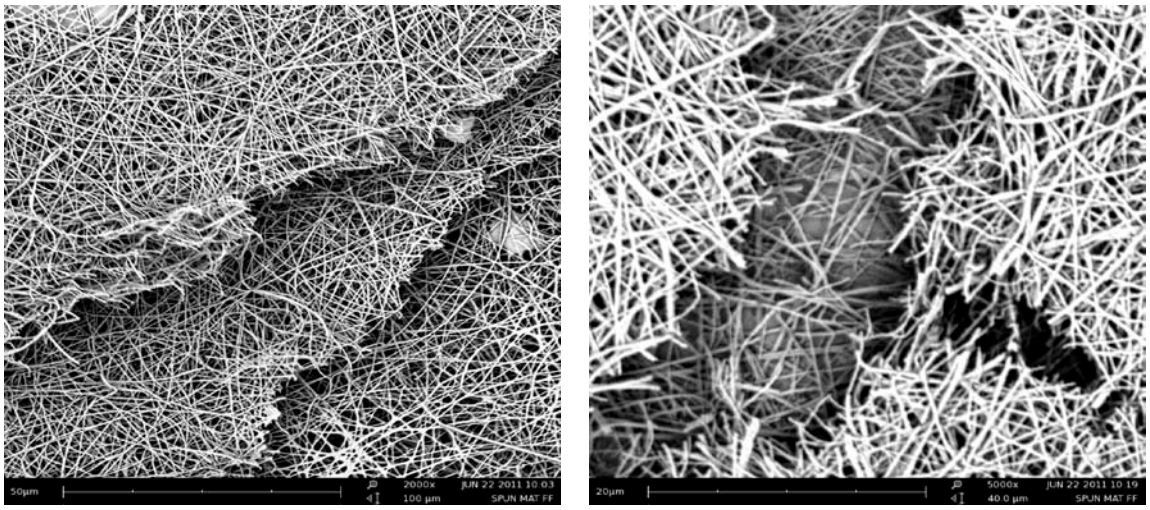

A B

**Figure 4.11:** SEM images of freeze fracture of spun mat derived from s(8PAA/DMF)c(4CS/30FA)
A, B, C (*2,000x, 5,000x* respectively)
Spinning conditions see Table 4.5

However, FEI SEM fails to give details regarding single fiber cross section. As the magnification exceeded 10,000x, the images became blurred.

These fibers were further investigated with FESEM. All samples were mounted on stage titled with 45 degree in advance for the purpose of capturing cross section. In Figures 4.12 and 4.13, little fuzzy dots were scattered at surface of fibers due to clustering of the Au-Pt coating. It was also found that the fibers drifted in the ion beam, because of the interaction between the beam and the ionizable groups on the polymers.

In both trials (Figures 4.12 and 4.13), the cross sections, cut by blade, were not flat, showing small cavities in the center. Since no evident fibrous structure extended from the core of the fibers that distinguished from sheath, we failed to confirm the presence of the core-sheath configuration. In addition, interfaces were not able to be detected due to the

metal coating (100 Å) for the purpose of conducting away the excess electrons, and preventing the sample from accumulating a negative charge. Signals from secondary electrons, which originated from a few nanometers of sample surface, only reflect the coated surface topography. While the backscattered electron, which is insensitive to light elements (low atomic number), is unable to differentiate the chemical compositions of the two polymers as well as the likely two layers[71].


**Figure 4.12:** SEM image of cross section of electrospun fibers derived from s(8PAA/DMF)c(5CS/dHCl)

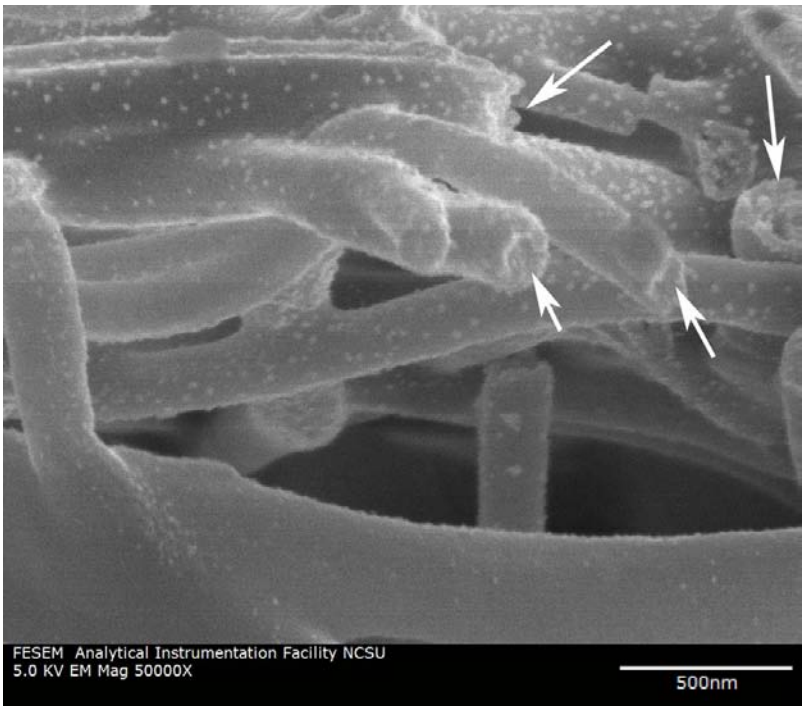


**Figure 4.13:** SEM image of cross section of electrospun fibers derived from s(8PAA/DMF)c(4CS/30FA)

## 4.5 Microtome and TEM

Doping bromophenol in core solution for increasing contrast of the interfaces may fail due to diffusion of the additive in the spinning process, misguiding the actual structure. Instead, slices of the product, electrospun mat derived from s(8PAA/DMF)c(4CS/30FA), were prepared, and then mounted onto copper grids for TEM characterization. These procedures were implemented by microtome, including resin with Epon for fiber fixation, and sectioning for obtaining longitudinal fiber samples as well as their cross sections. The thickness of each slice is approximately 100 nm.

If patterns of two concentric circles with distinguishable contrast were found in fiber cross sections under TEM resulting from different density of each component, the core-sheath structure will prove true.

However, even operated at 80 kV which is the lowest power of the TEM instrument, the beam quickly damaged the slice, making it split and melt. Dark fibrous structures at nano-scale were hardly observed which may correspond to the fibers embedded in surrounding matrix (Figure 4.14). The sample further vaporized when we refocused on it. Neither detailed longitudinal structures nor cross sections of fibers were captured. Therefore, core-sheath structure is inconclusive.

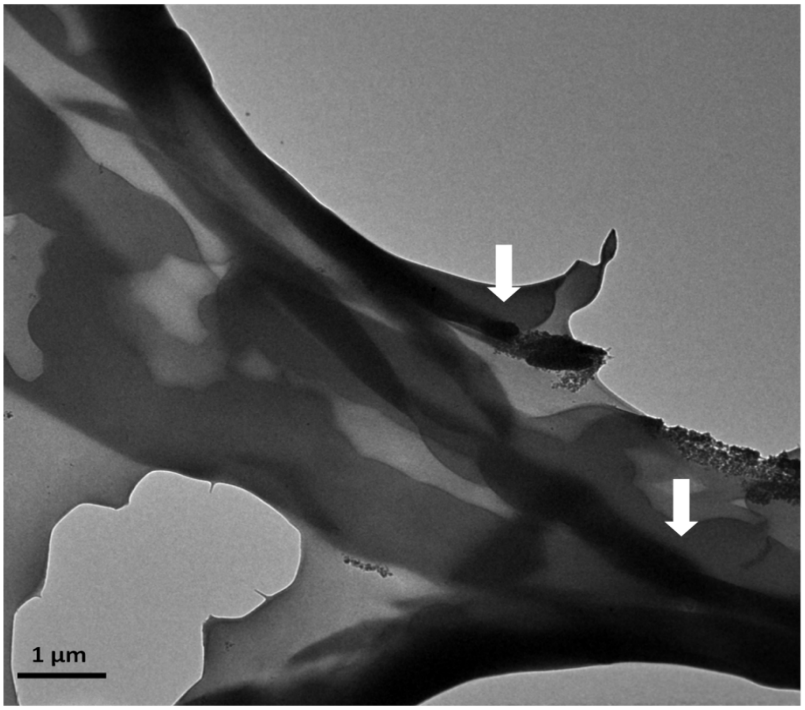


**Figure 4.14:** TEM image of electrospun fibers embedded in Epon derived from s(8PAA/DMF)c(4CS/30FA)

## 4.6 FTIR Analysis

Since the morphologies of electrospun mats derived from s(8PAA/DMF)c(4CS/30FA) before and after exposure to water are relatively uniform, this mat and its complex were chosen for infrared characterization. The results concerning chemical compositions of the products would reveal the interactions among the two polyelectrolytes, explaining its structural stability in water.

Figure 4.15 displays the FTIR spectra of pure PAA and chitosan powders, electrospun PAA-CS mat and its complex after soaking, illustrating the chemical compositions of a top thin layer (around 1μm) in each sample[72]. Since the average diameter of the electrospun fibers was around 200 nm, several layers of stacking would meet the FTIR testing demand.

The spectrum of electrospun mat (purple) is similar to that of pure PAA powder (light blue), yet several new bands were detected. They confirm the chitosan inside the mat, corresponding to its finger print region (around 1060 $cm^{-1}$), characteristic peaks (Amide I band at 1653 $cm^{-1}$ and the amide II band at 1592 $cm^{-1}$) and N-H single bond (around 3400 $cm^{-1}$ ) (Figure 4.15) [73].

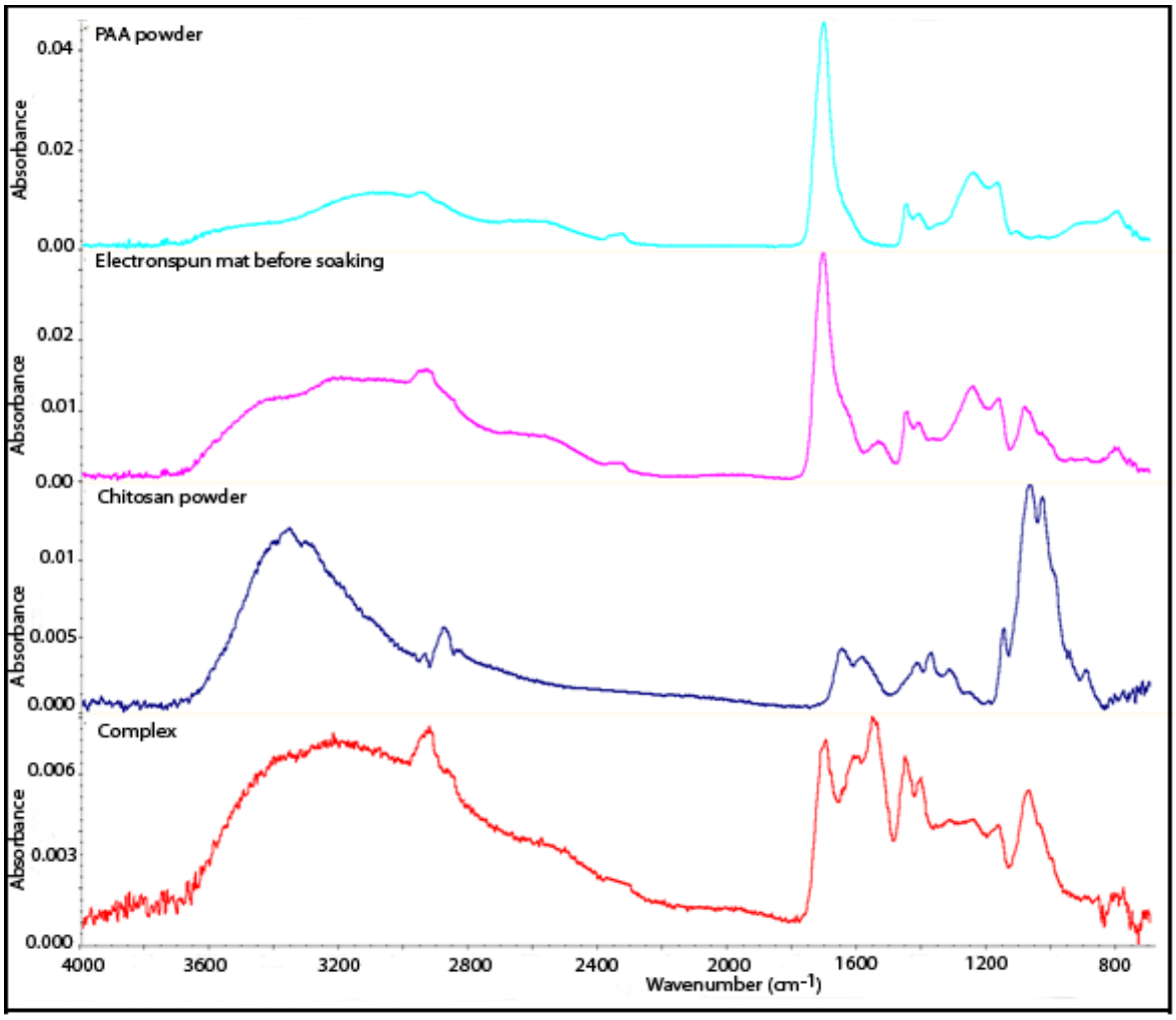


**Figure 4.15:** FTIR spectra of pure PAA powder (light blue), chitosan powder (dark blue), electrospun mat derived from s(8PAA/DMF)c(4CS/30FA) (purple) and its complex after soaking (red)

Shown in Figure 4.16, intensity of absorption bands of PAA appear around 1701 $cm^{-1}$, and 1452 $cm^{-1}$, which can be assigned to carboxyl groups[74], decreased sharply in the spectrum of the complex compared to its mat before soaking, which means large amount of PAA were removed dissolving in water.

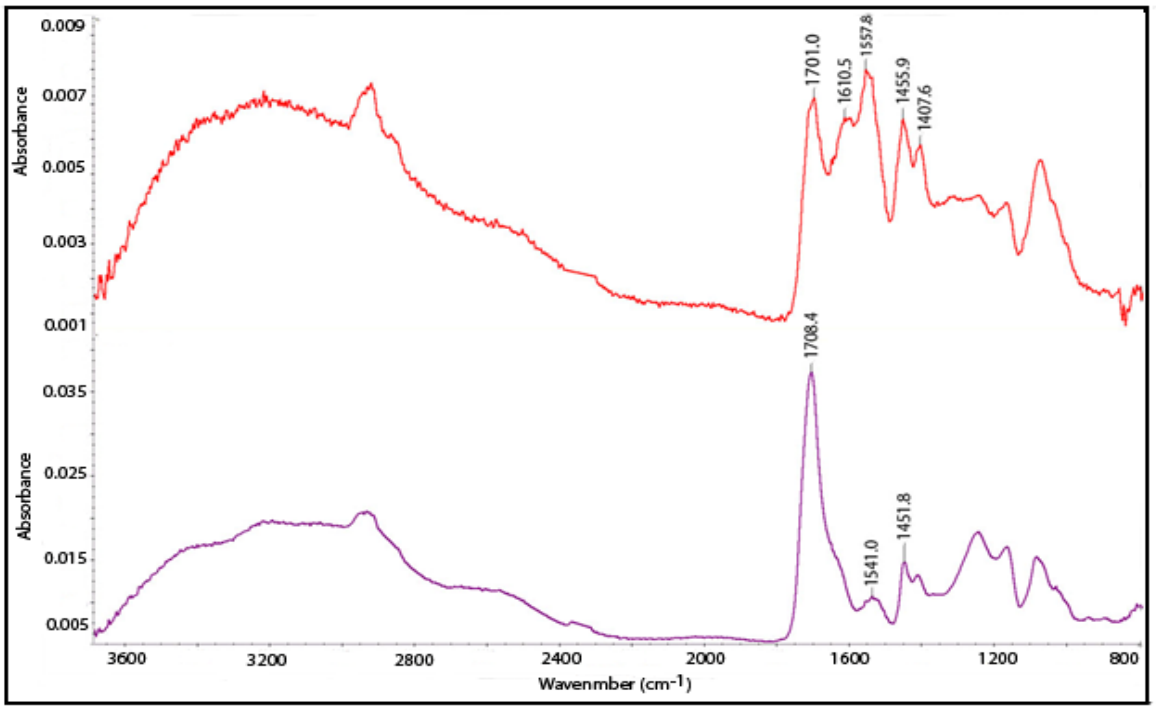


**Figure 4.16:** FTIR spectra for electrospun mat derived from s(8PAA/DMF)c(4CS/30FA) (purple) and its complex after soaking (red)

In Figure 4.17, a significant new peak shows up at 1558 $cm^{-1}$ after soaking in D.I. water (~ pH 7), corresponding to the absorption characteristics of $NH_3^+$ and $COO^-$ groups[70]. In addition, two peaks at 1611 $cm^{-1}$ and 1407 $cm^{-1}$ confirm the presence of $COO^-$ in PAA and $NH_3^+$ in chitosan, respectively[75].

These results demonstrate that carboxylic groups of PAA residue dissociated into $COO^-$, interacting with $NH_3^+$ of chitosan via electrostatic interactions. Therefore, polyelectrolyte complexes formed the insoluble residue, whereas PAA dominated the components that composed of the electrospun mat before rinse.

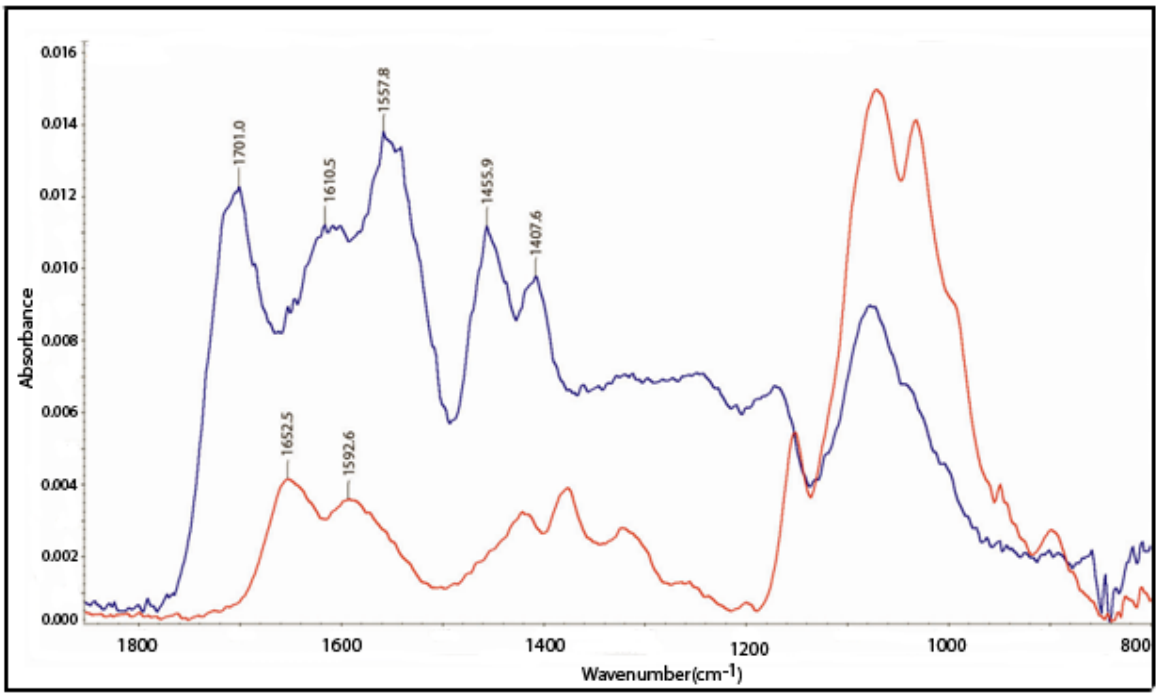


**Figure 4.17:** Expanded FTIR spectra for chitosan powder (red) and complex derived from s(8PAA/DMF)c(4CS/30FA) (blue)

# 5. CONCLUSIONS AND FUTURE WORK

In this work, bicomponent complexes composed of chitosan and poly(acrylic acid) (PAA) have been generated via coaxial electrospinnig, in which chitosan, a difficult-to-electrospin polymer, was induced to spin by the sheath material PAA and fibrous structures were formed. We focused on seeking desirable solvent combinations that allows the fiber formation process successful. PAA/dimethylformamide (DMF) was consistently employed as sheath solution, while chitosan was dissolved in four different solvents, including 90% aqueous acetic acid (90HAc), 90% aqueous formic acid (90FA), 1% hydrochloric acid (dHCl) and 30% aqueous formic acid (30FA). The first two solvents, 90HAc and 90FA, did not result in fiber formation. When 90HAc was used as core solvent, gelation occurred, which led to no jet formation; whereas 90FA resulted in interfacial diffusion, disrupting original electrospinable sheath solution. Although the other two solutions spun, different morphologies of the resulting mats were observed under SEM. dHCl as core solvent resulted in unsatisfactory drying. Wet fiber interlaced and the mat appeared film-like. So far, 30FA is the best core solvent for producing uniform fibers.

For studying structural stability of fibrous complex, both mats were rinsed in distilled water overnight, and swelled. Distinguishable fibers covered with nano-beads were observed in 30FA case. The rough surface, which may due to the interfacial diffusion, is advantageous to increase surface/area volume. In contrast, the morphology of the other mat derived from dHCl was rather random showing solid films coexisting with porous matrix.

Nanofibrous mats derived from 30FA and dHCl core solvent systems were cut with sharp blade at 77 K, but no distinct interfaces were observed because of the contrast

mechanism of scanning electron microscopy (SEM). Secondary electrons are just able to provide signals from sample surfaces originated from metal coating. While backscattering electrons, which are atom number (Z) sensitive, fail to differentiate the light elements in PAA or chitosan and characterize the interface. High-power transmission electron microscopy (TEM) damaged the slice prepared by microtome, resulting in inconclusive core-sheath structure. Finally, FTIR data showed the chemical compositions of the electrospun mat and its complex derived from 30FA as core solvent system. Though chitosan was detected, PAA was confirmed as the major component in the electropsun fibers before soaking. Characteristic peak at 1558 $cm^{-1}$ demonstrated the presence of $COO^-$ and $NH_3^+$ interaction, and revealed the polyelectrolyte complexes were the insoluble material after rinse.

In general, other than thermal induced phase transformation or post chemical treatment, coaxial electrospinnig prove to be a novel approach and efficient way of fabricating porous polyelectrolyte complexes at the nano-scale.

In future work, we look forward to optimizing material and processing parameters to improve the consistency of the product. For spinning conditions, if a higher voltage can be applied, the tip-to-collector distance can be increased without influencing electrical strength, providing more space for solvent evaporation. The density of fibers seems to be relevant to the complexes morphologies after rinsing, an advanced collector, such as rotating drum, might be preferred. It could control the inter-fiber porosity to some extent, which may facilitate creating controllable swollen structure at the nanoscle. Varying solution compositions would be an alternative way to solve the difficulty in evaporation, for example adding volatile solvent.

With all these in mind, significant breakthroughs would be using coaxial electrospinning to fabricate nanofibrous complexes consisting of a more biocompatible polyelectrolyte, like chitosan or heparin, at sheath while an oppositely charged polymer in core, which greatly expand the potentials of this technique.

Further characterizations are in demand to elucidate the structure of the electrospun mat as well as their complexes in my work. An appropriate transmission electron microscopy (TEM) could be used to find and observe the likely interface, especially from the cross section of the fibers. Moreover, to detect the surface composition as well as sheath thickness, x-ray photoelectron spectroscopy (XPS) could be utilized for depth profile. Other area of focus include, the structure-property relationships of the end product, cell proliferation properties and biodegradability particularly in buffer, and other potential applications in anti-corrosion coating and drug delivery.

# 6. REFERENCES


[1] Kujawa, P.; Schmauch, G.; Viitala, T.; Badia, A.; Winnik, F.M. Construction of Viscoelastic Biocompatible Films Via the Layer-by-Layer Assembly of Hyaluronan and Phosphorylcholine-Modified Chitosan. Biomacromolecules **2007**, *8*, 3169-3176.

[2] Xie, J.; Li, X.; Xia, Y. Putting Electrospun Nanofibers to Work for Biomedical Research. Macromolecular Rapid Communications **2008**, *29*, 1775-1792.

[3] Li, Q.; Dunn, E.T.; Grandmaison, E.W.; Goosen, M.F.A. Applications and Properties of Chitosan. Journal of Bioactive and Compatible Polymers **1992**, *7*, 370-397.

[4] Li, Z.F.; Ruckenstein, E. Water-Soluble Poly(Acrylic Acid) Grafted Luminescent Silicon Nanoparticles and their use as Fluorescent Biological Staining Labels. Nano Letters **2004**, *4*, 1463-1467.

[5] Yang, S.; Fu, Y.; Jeong, S.H.; Park, K. Application of Poly(Acrylic Acid) Superporous Hydrogel Microparticles as a Super-Disintegrant in Fast-Disintegrating Tablets. J. Pharm. Pharmacol. **2004**, *56*, 429-436.

[6] Queen, H. Electrospinning Chitosan-Based Nanofibers for Biomedical Applications **2006**.

[7] Penchev, H.; Paneva, D.; Manolova, N.; Rashkov, I. Novel Electrospun Nanofibers Composed of Polyelectrolyte Complexes. Macromolecular Rapid Communications **2008**, *29*, 677-681.

[8] Dobrynin, A.V.; Rubinstein, M. Theory of Polyelectrolytes in Solutions and at Surfaces. Progress in Polymer Science **2005**, *30*, 1049-1118.

[9] Beachley, V.; Wen, X. Polymer Nanofibrous Structures: Fabrication, Biofunctionalization, and Cell Interactions. Progress in Polymer Science **2010**, *35*, 868-892.

[10] Schiffman, J.D.; Schauer, C.L. A Review: Electrospinning of Biopolymer Nanofibers and their Applications. Polymer Reviews **2008**, *48*, 317-352.

[11] Ma, Z.; Kotaki, M.; Ramakrishna, S. Electrospun Cellulose Nanofiber as Affinity Membrane. J. Membr. Sci. **2005**, *265*, 115-123.

[12] Huang, Z.; Zhang, Y.; Kotaki, M.; Ramakrishna, S. A Review on Polymer Nanofibers by Electrospinning and their Applications in Nanocomposites. Composites Sci. Technol. **2003**, *63*, 2223-2253.

[13] Chua, K.; Chai, C.; Lee, P.; Tang, Y.; Ramakrishna, S.; Leong, K.W.; Mao, H. Surface-Aminated Electrospun Nanofibers Enhance Adhesion and Expansion of Human Umbilical Cord Blood Hematopoietic stem/progenitor Cells. Biomaterials **2006**, *27*, 6043-6051.

[14] Hartgerink, J.D.; Beniash, E.; Stupp, S.I. Self-Assembly and Mineralization of Peptide-Amphiphile Nanofibers. Science **2001**, *294*, 1684-1688.

[15] Lee, O.; Stupp, S.I.; Schatz, G.C. Atomistic Molecular Dynamics Simulations of Peptide Amphiphile Self-Assembly into Cylindrical Nanofibers. J. Am. Chem. Soc. **2011**, *133*, 3677-3683.

[16] van de Witte, P.; Dijkstra, P.J.; van den Berg, J.W.A.; Feijen, J. Phase Separation Processes in Polymer Solutions in Relation to Membrane Formation. J. Membr. Sci. **1996**, *117*, 1-31.

[17] Zhao, J.; Han, W.; Chen, H.; Tu, M.; Zeng, R.; Shi, Y.; Cha, Z.; Zhou, C. Preparation, Structure and Crystallinity of Chitosan Nano-Fibers by a solid–liquid Phase Separation Technique. Carbohydr. Polym. **2011**, *83*, 1541-1546.

[18] Feng, L.; Li, S.; Li, H.; Zhai, J.; Song, Y.; Jiang, L.; Zhu, D. Super-Hydrophobic Surface of Aligned Polyacrylonitrile Nanofibers. Angewandte Chemie **2002**, *114*, 1269-1271.

[19] Agarwal, S.; Wendorff, J.H.; Greiner, A. Use of Electrospinning Technique for Biomedical Applications. Polymer **2008**, *49*, 5603-5621.

[20] Deitzel, J.M.; Kleinmeyer, J.; Harris, D.; Beck Tan, N.C. The Effect of Processing Variables on the Morphology of Electrospun Nanofibers and Textiles. Polymer **2001**, *42*, 261-272.

[21] Moghe, A.K.
Core-Sheath Differentially Biodegradable Nanofiber Structures for Tissue Engineering. **2008**.

[22] Megelski, S.; Stephens, J.S.; Chase, D.B.; Rabolt, J.F. Micro- and Nanostructured Surface Morphology on Electrospun Polymer Fibers. Macromolecules **2002**, *35*, 8456-8466.

[23] Choi, J.S.; Lee, S.W.; Jeong, L.; Bae, S.; Min, B.C.; Youk, J.H.; Park, W.H. Effect of Organosoluble Salts on the Nanofibrous Structure of Electrospun Poly(3-Hydroxybutyrate-Co-3-Hydroxyvalerate). Int. J. Biol. Macromol. **2004**, *34*, 249-256.

[24] Reneker, D.H.; Yarin, A.L.; Fong, H.; Koombhongse, S. Bending Instability of Electrically Charged Liquid Jets of Polymer Solutions in Electrospinning. J. Appl. Phys. **2000**, *87*, 4531.

[25] Sill, T.J.; von Recum, H.A. Electrospinning: Applications in Drug Delivery and Tissue Engineering. Biomaterials **2008**, *29*, 1989-2006.

[26] Geng, X.; Kwon, O.; Jang, J. Electrospinning of Chitosan Dissolved in Concentrated Acetic Acid Solution. Biomaterials **2005**, *26*, 5427-5432.

[27] Vrieze, S.D.; Westbroek, P.; Camp, T.V.; Langenhove, L.V. Electrospinning of Chitosan Nanofibrous Structure: Feasibility Study. J. Mater. Sci **2007**, *42*, 8029.

[28] Ohkawa, K.; Cha, D.; Kim, H.; Nishida, A.; Yamamoto, H. Electrospinning of Chitosan. Macromolecular Rapid Communications **2004**, *25*, 1600-1605.

[29] Ohkawa, K.; Minato, K.; Kumagai, G.; Hayashi, S.; Yamamoto, H. Chitosan Nanofiber. Biomacromolecules **2006**, *7*, 3291-3294.

[30] Duan, B.; Dong, C.; Yuan, X.; Yao, K. Electrospinning of Chitosan Solutions in Acetic Acid with Poly(Ethylene Oxide). Journal of Biomaterials Science -- Polymer Edition **2004**, *15*, 797-811.

[31] Tong Lin, e.a. Using Chitosan as a Thickener for Electrospinning Dilute PVA Solutions to Improve Fibre Uniformity. Nanotechnology **2006**, *17*, 3718.

[32] Zhang, J.; Yang, D.; Xu, F.; Zhang, Z.; Yin, R.; Nie, J. Electrospun Coreâˆ'Shell Structure Nanofibers from Homogeneous Solution of Poly(Ethylene Oxide)/Chitosan. Macromolecules **2009**, *42*, 5278-5284.

[33] Um, I.C.; Fang, D.; Hsiao, B.S.; Okamoto, A.; Chu, B. Electro-Spinning and Electro-Blowing of Hyaluronic Acid. Biomacromolecules **2004**, *5*, 1428-1436.

[34] Uppal, R.; Ramaswamy, G.N.; Arnold, C.; Goodband, R.; Wang, Y. Hyaluronic Acid Nanofiber Wound dressing—production, Characterization, and in Vivo Behavior. JOURNAL OF BIOMEDICAL MATERIALS RESEARCH B **2010**, *97B.*

[35] Viswanathan, G.; Murugesan, S.; Pushparaj, V.; Nalamasu, O.; Ajayan, P.M.; Linhardt, R.J. Preparation of Biopolymer Fibers by Electrospinning from Room Temperature Ionic Liquids. Biomacromolecules **2006**, *7*, 415-418.

[36] Casper, C.L.; Yamaguchi, N.; Kiick, K.L.; Rabolt, J.F. Functionalizing Electrospun Fibers with Biologically Relevant Macromolecules. Biomacromolecules **2005**, *6*, 1998-2007.

[37]Http://www.Sigmaaldrich.com/catalog/Lookup.do?N5=All&N3=mode+matchpartialmax&N4=polyacrylic+acid&D7=0&D10=polyacrylic+acid&N1=S_ID&ST=RS&N25=0&F=PR.

[38] Khanam, N.; Mikoryak, C.; Draper, R.K.; Balkus Jr., K.J. Electrospun Linear Polyethyleneimine Scaffolds for Cell Growth. Acta Biomaterialia **2007**, *3*, 1050-1059.

[39] Li, L.; Hsieh, Y. Ultra-Fine Polyelectrolyte Fibers from Electrospinning of Poly(Acrylic Acid). Polymer **2005**, *46*, 5133-5139.

[40] Chunder, A.; Sarkar, S.; Yu, Y.; Zhai, L. Fabrication of Ultrathin Polyelectrolyte Fibers and their Controlled Release Properties. Colloids and Surfaces B: Biointerfaces **2007**, *58*, 172-179.

[41] Dubas, S.T.; Schlenoff, J.B. Polyelectrolyte Multilayers Containing a Weak Polyacid:â€‰ Construction and Deconstruction. Macromolecules **2001**, *34*, 3736-3740.

[42] Moghe, A.K.; Gupta, B.S. Co-Axial Electrospinning for Nanofiber Structures: Preparation and Applications. Polymer Reviews **2008**, *48*, 353-377.

[43] Zhuo, H.T.; Hu, J.L.; Chen, S.J. Coaxial Electrospun Polyurethane Core-Shell Nanofibers for Shape Memory and Antibacterial Nanomaterials. eXPRESS Polymer Letters **2011**, *5*, 182-187.

[44] Zhang, Y.Z.; Venugopal, J.; Huang, Z.-.; Lim, C.T.; Ramakrishna, S. Characterization of the Surface Biocompatibility of the Electrospun PCL-Collagen Nanofibers using Fibroblasts. Biomacromolecules **2005**, *6*, 2583-2589.

[45] Hayati, I.; Bailey, A.I.; Tadros, T.F. Investigations into the Mechanisms of Electrohydrodynamic Spraying of Liquids : I. Effect of Electric Field and the Environment on Pendant Drops and Factors Affecting the Formation of Stable Jets and Atomization. J. Colloid Interface Sci. **1987**, *117*, 205-221.

[46] Stanger, J. Charge Transfer Mechanism in Electrospinning. **2008**.

[47] Li, D.; Xia, Y. Direct Fabrication of Composite and Ceramic Hollow Nanofibers by Electrospinning. Nano Letters **2004**, *4*, 933-938.

[48] Zhang, Y.Z.; Wang, X.; Feng, Y.; Li, J.; Lim, C.T.; Ramakrishna, S. Coaxial Electrospinning of (Fluorescein Isothiocyanate-Conjugated Bovine Serum Albumin)-Encapsulated Poly(Caprolactone) Nanofibers for Sustained Release. Biomacromolecules **2006**, *7*, 1049-1057.

[49] Kumar, A., Ed.*Nanofibers*.; INTECH, Croatia, 2010; pp. 438.

[50] Díaz, J.?.; Barrero, A.; Márquez, M.; Loscertales, I.?. Controlled Encapsulation of Hydrophobic Liquids in Hydrophilic Polymer Nanofibers by Co-Electrospinning. Advanced Functional Materials **2006**, *16*, 2110-2116.

[51] Kurban, Z.; Lovell, A.; Bennington, S.M.; Jenkins, D.W.K.; Ryan, K.R.; Jones, M.O.; Skipper, N.T.; David, W.I.F. A Solution Selection Model for Coaxial Electrospinning and its Application to Nanostructured Hydrogen Storage Materials. The Journal of Physical Chemistry C **2010**, *114*, 21201-21213.

[52] Ojha, S.S.; Stevens, D.R.; Hoffman, T.J.; Stano, K.; Klossner, R.; Scott, M.C.; Krause, W.; Clarke, L.I.; Gorga, R.E. Fabrication and Characterization of Electrospun Chitosan Nanofibers Formed Via Templating with Polyethylene Oxide. Biomacromolecules **2008**, *9*, 2523-2529.

[53] Zhang, Y.; Huang, Z.; Xu, X.; Lim, C.T.; Ramakrishna, S. Preparation of Coreâˆ'Shell Structured PCL-r-Gelatin Bi-Component Nanofibers by Coaxial Electrospinning. Chemistry of Materials **2004**, *16*, 3406-3409.

[54] He, C.; Huang, Z.; Han, X.; Liu, L.; Zhang, H.; Chen, L. Coaxial Electrospun Poly(Lactic Acid) Ultrafine Fibers for Sustained Drug Delivery. Journal of Macromolecular Science, Part B **2006**, *45*, 515-524.

[55] Yu, J.; Fridrikh, S.; Rutledge, G. Production of Submicrometer Diameter Fibers by Two-Fluid Electrospinning. Adv Mater **2004**, *16*, 1562-1566.

[56] Sun, Z.; Zussman, E.; Yarin, A.L.; Wendorff, J.H.; Greiner, A. Compound Core?Shell Polymer Nanofibers by Co-Electrospinning. Adv Mater **2003**, *15*, 1929-1932.

[57] Bognitzki, M.; Hou, H.; Ishaque, M.; Frese, T.; Hellwig, M.; Schwarte, C.; Schaper, A.; Wendorff, J.H.; Greiner, A. Polymer, Metal, and Hybrid Nano- and Mesotubes by Coating Degradable Polymer Template Fibers (TUFT Process). Adv Mater **2000**, *12*, 637-640.

[58] Caruso, R.A.; Schattka, J.H.; Greiner, A. ChemInform Abstract: Titanium Dioxide Tubes from Sol-Gel Coating of Electrospun Polymer Fibers. ChemInform **2001**, *32*, no-no.

[59] Dror, Y.; Salalha, W.; Avrahami, R.; Zussman, E.; Yarin, A.?.; Dersch, R.; Greiner, A.; Wendorff, J.?. One-Step Production of Polymeric Microtubes by Co-Electrospinning. Small **2007**, *3*, 1064-1073.

[60] Jiang, H.; Hu, Y.; Li, Y.; Zhao, P.; Zhu, K.; Chen, W. A Facile Technique to Prepare Biodegradable Coaxial Electrospun Nanofibers for Controlled Release of Bioactive Agents. J. Controlled Release **2005**, *108*, 237-243.

[61] Loscertales, I.G.; Barrero, A.; MÃ¡rquez, M.; Spretz, R.; Velarde-Ortiz, R.; Larsen, G. Electrically Forced Coaxial Nanojets for One-Step Hollow Nanofiber Design. J. Am. Chem. Soc. **2004**, *126*, 5376-5377.

[62] Li, D.; McCann, J.; Xia, Y. Use of Electrospinning to Directly Fabricate Hollow Nanofibers with Functionalized Inner and Outer Surfaces. Small **2005**, *1*, 83-86.

[63] Wei, M.; Lee, J.; Kang, B.; Mead, J. Preparation of Core-Sheath Nanofibers from Conducting Polymer Blends. Macromolecular Rapid Communications **2005**, *26*, 1127-1132.

[64] Yu, D.; Branford-White, C.; Chatterton, N.P.; White, K.; Zhu, L.; Shen, X.; Nie, W. Electrospinning of Concentrated Polymer Solutions. Macromolecules **2010**, *43*, 10743-10746.

[65] El-Tahlawy, K.; Hudson, S.M. Chitosan: Aspects of Fiber Spinnability. J Appl Polym Sci **2006**, *100*, 1162-1168.

[66] Wang, W.; Bo, S.; Li, S.; Qin, W. Determination of the Mark-Houwink Equation for Chitosans with Different Degrees of Deacetylation. Int. J. Biol. Macromol. **1991**, *13*, 281-285.

[67] Wang, W.; Qin, W.; Bo, S. Influence of the Degree of Deacetylation of Chitosan on its Mark-Houwink Equation Parameters. Die Makromolekulare Chemie, Rapid Communications **1991**, *12*, 559-561.

[68] Chavasit, V.; Kienzle-Sterzer, C.; Torres, J.A. Formation and Characterization of an Insoluble Polyelectrolyte Complex: Chitosan-Polyacrylic Acid. Polymer Bulletin **1988**, *19*, 223-230.

[69] Http://encyclopedia.Airliquide.com/Encyclopedia.Asp?GasID=17.

[70] De Lima, M.S.P.; Freire, M.S.; Fonseca, J.L.C.; Pereira, M.R. Chitosan Membranes Modified by Contact with Poly(Acrylic Acid). Carbohydr. Res. **2009**, *344*, 1709-1715.

[71] Http://en.Wikipedia.org/wiki/Scanning_electron_microscope.

[72] Http://wenku.Baidu.com/view/3a7c46d850e2524de5187e61.Html.

[73] Hu, Y.; Jiang, X.; Ding, Y.; Ge, H.; Yuan, Y.; Yang, C. Synthesis and Characterization of Chitosan-Poly(Acrylic Acid) Nanoparticles. Biomaterials **2002**, *23*, 3193-3201.

[74] Nge, T.T.; Yamaguchi, M.; Hori, N.; Takemura, A.; Ono, H. Synthesis and Characterization of chitosan/poly(Acrylic Acid) Polyelectrolyte Complex. J Appl Polym Sci **2002**, *83*, 1025-1035.

[75] Nam, S.Y.; Lee, Y.M. Pervaporation and Properties of Chitosan-Poly(Acrylic Acid) Complex Membranes. J. Membr. Sci. **1997**, *135*, 161-171.

[76]http://www.smartmeasurement.com/en/wizards/flowmeter/flmtr_mag_conductivity.asp

# APPENDICES

# APPENDIX A

Before finally deciding on the core material, other combinations were studied to determine the optimal processing parameters for our coaxial electrospinning setup.

## A.1 Materials

Two poly(ethylene oxide) (PEO) samples with molecular weights of approximate 900,000 and 400,000 g/mol respectively were purchased from Scientific Polymer. Polyethyleneimine (PEI) solution, 50% (w/v) in water, was purchased from Fluka.

## A.2 Effect of feed rates

In order to study the fibrous morphologies as a function of throughput, two readily electrospinable polymers solutions were employed. Poly(acrylic acid) PAA/ dimethylformamide (DMF) solution was consistently used as sheath solution with a fixed throughput, while the feed rate of core solution, PEO in deionized water (D.I. water), was varied. The processing parameters are shown in Table 7.1

**Table A.1:** Coaxial electrospinning conditions for sPAAcPEO

| trial | Sheath solution | Core solution | Sheath feed rater (μL/min) | Core feed rate (μL/min) | Tip to collector distance (cm) | Applied voltage (kV) |
|---|---|---|---|---|---|---|
| 1 | 8% PAA in DMF | 4% PEO(900k) in D.I. water | 10 | 2 | 15 | 15 |
| 2 | | | | 6 | | |

Both trials were able to readily generated fibers. Due to different core feed rate, SEM images show that the two electrospun mats are different in microsturcture. Fibrous morphology is clearly observed along with a few random clots, when core feed rate was 2 μL/min. As it increased to 6 μL/min, the mat appeared film-like. The solvents in that case were not effectively evaporated, making the wet fiber fused structure.

Considering 2 μL/min might be too low to supply enough core material for complex generation, we set the core feed rate as 6 μL/min for further trials while increasing the tip-to-collector distance to provide more space for fiber solidification.

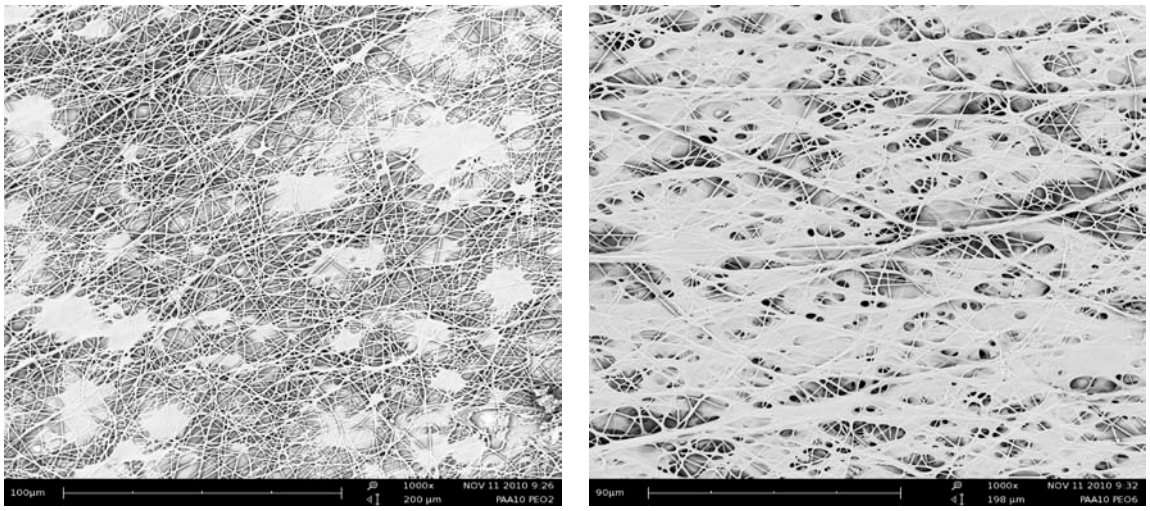


**Figure A.1:** SEM images of bicomponent composite consisted of PAA as sheath and PEO as core, sheath feed rate was fixed at 10 μL/min, while core feed rate was (A) 2 μL/min, and (B) 6 μL/min, respectively
Spinning conditions see Table A.1

## A.3 Effect of polymer charging

Khanam, et al. successfully electrospun linear PEI they synthesized, whereas the commercial one failed to spin although they attempted it[38]. We decided to blend the commercial PEI aqueous solution with PEO, a readily electrospinable polymer, to assist the process.

The first attempt, which was to dissolve PEO powder directly into aqueous PEI, was in vain, perhaps because PEO is immiscible with slightly charged PEI. The PEO powder formed micelles that survived for a long time without absolute dissolution.

With this in mind, 6% PEO (400k) aqueous solutions were prepared beforehand and blended with commercial PEI aqueous solution. These mixtures were transparent to the eye without any apparent flocculation.

**Table A.2:** PEI/PEO solutions compositions and their acidic value

| Solution code | Blend ratio<br>50% PEI sol. (g)/<br>6% PEO (400k) sol.(g)/<br>extra deionized water(g) | Added 37% hydrochloric acid (HCl) volume (mL) | Corresponding solution pH |
|---|---|---|---|
| 6PEIb4PEO | 3 : 16.6 : 5.4,<br>(10% polymers in 25 g solution (6% PEI + 4% PEO)) | 0 | 10.0 |
| 6PEIb4PEO(0.6H) | | 0.6 | 10.0 |
| 6PEIb4PEO(1.2H) | | 1.2 | 2.0 |
| 6PEIb4PEO(1.8H) | | 1.8 | 1.0 |

**Table A.3:** Electrospinning conditions of PEI/PEO blend

| Solution | Feed rate (μL/min) | Apply Voltage (kV) | Tip to collector distance (cm) |
|---|---|---|---|
| 6PEIb4PEO | 10 | 15 | 15 |
| 6PEIb4PEO(1.5H) | 10 | 15 | 15 |

pH of 6PEIb4PEO solution is higher than 7, which indicates that PEI naturally absorbs hydrogen ions ($H^+$) from water. Indeed, the bonding sites originated from amino group were far from saturated in this solution. pH value of this solution did not change as small amount of concentrated HCl was added (Table 7.2). Keeping adding concentrated HCl to pH=2, amino groups are fully positively charged[40].

These two solutions, 6PEIb4PEO and 6PEIb4PEO(1.2H), were chosen to study the effect of charge on fiber formation. The polymer jet stream derived from 6PEIb4PEO could consistently maintain its stability, similar to that of spinning PEO aqueous solution. The resulted fibers show high distributions and numerous branches (Fig 7.2 A, B). When 6PEIb4PEO(1.2H) (pH=2) was electrospun, an interesting scenario happened. The product, charged fibrous mat, partially adhered to the foil was able to response to the electrical field, waving themselves toward to the tip of needle where is the highest potential. The messy product contained large bump and tiny fibers (Fig. 7.2 C, D).

Compared to uncharged polymers, the protonated PEI force the jets to form branches en route in order to dramatically increase surface area and decrease the charge density. Thus, network structures were observed. Spinning the highly acidic PEI solution, 6PEIb4PEO(1.2H), mechanical responses of the products corresponding to the electrical field is attributed to the reverse piezoelectric effect, which originated from nature of the highly polarized polymer, i.e. charged PEI.

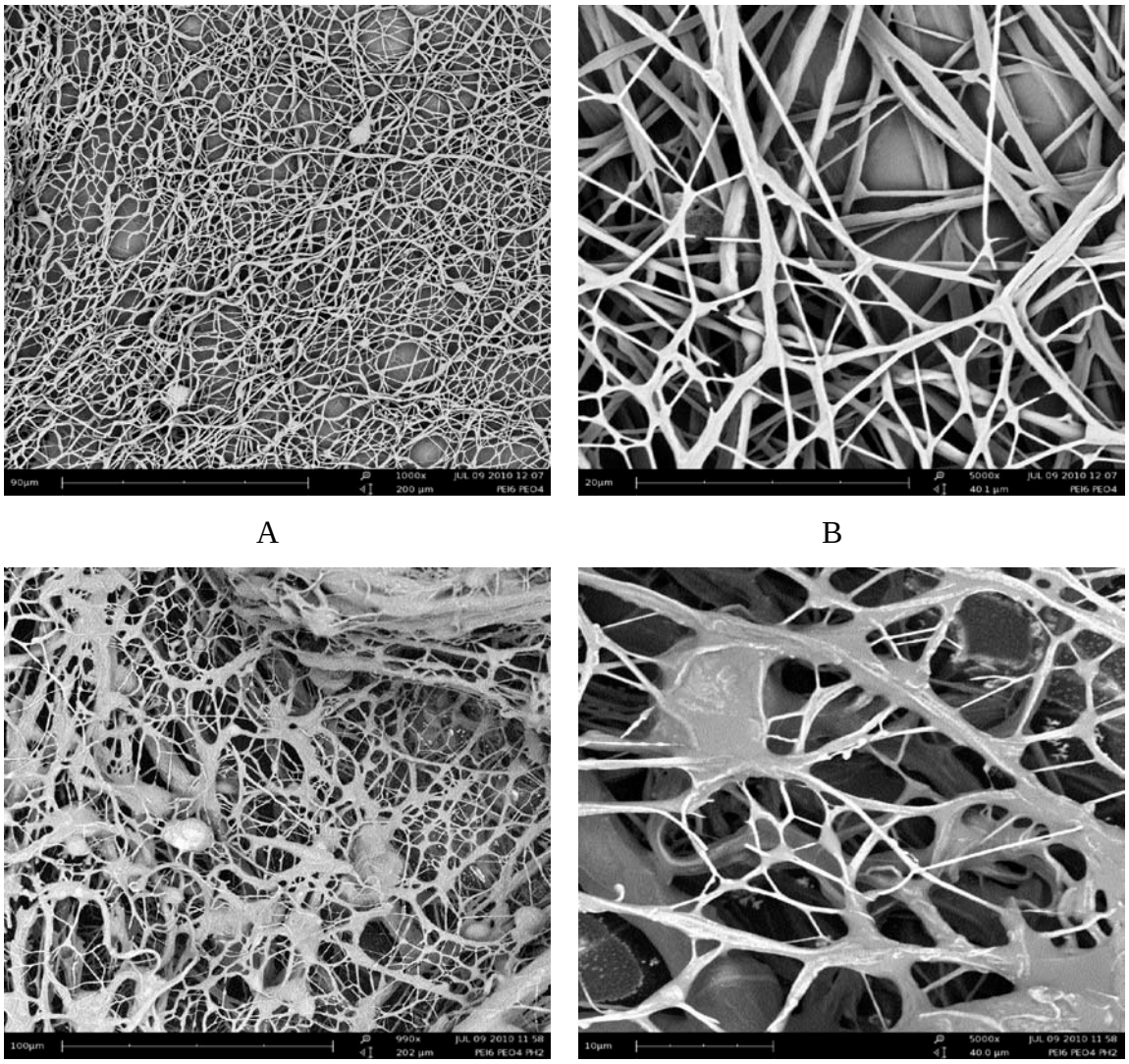

A B

C D

**Figure A.2:** Nanofiber generated from
6PEIb4PEO A*(1,000x)*, B*(5,000x)*
6PEIb4PEO(1.5HCl) C*(990x)*, D*(5,000x)*
Spinning conditions see Table A.3